(12) INTERNATIONAL APPLICATION PUBLISHED UNDER THE PATENT COOPERATION TREATY (PCT)

(19) World Intellectual Property Organization
International Bureau

(43) International Publication Date
12 September 2014 (12.09.2014)

WIPO | PCT

(10) International Publication Number
WO 2014/137750 A1

(51) International Patent Classification:
G06F 19/00 (2011.01)

(21) International Application Number:
PCT/US2014/019074

(22) International Filing Date:
27 February 2014 (27.02.2014)

(25) Filing Language: English

(26) Publication Language: English

(30) Priority Data:
61/773,360 6 March 2013 (06.03.2013) US
14/069,691 1 November 2013 (01.11.2013) US

(71) Applicant: **EXA CORPORATION** [US/US]; 55 Network Drive, Burlington, Massachusetts 01803 (US).

(72) Inventors: **PÉROT, Franck Léon**; 3139 Irving Street, San Francisco, California 94122 (US). **MANN, Adrien**; 1709 Shattuck Ave, #318, Berkeley, California 94709 (US). **FREED, David M.**; 173 Red Hawk Ct., Brisbane, California 94005 (US).

(74) Agent: **DRAKE, Tonya S.**; Fish & Richardson P.C., P.O. Box 1022, Minneapolis, Minnesota 55440-1022 (US).

(81) Designated States *(unless otherwise indicated, for every kind of national protection available)*: AE, AG, AL, AM, AO, AT, AU, AZ, BA, BB, BG, BH, BN, BR, BW, BY, BZ, CA, CH, CL, CN, CO, CR, CU, CZ, DE, DK, DM, DO, DZ, EC, EE, EG, ES, FI, GB, GD, GE, GH, GM, GT, HN, HR, HU, ID, IL, IN, IR, IS, JP, KE, KG, KN, KP, KR, KZ, LA, LC, LK, LR, LS, LT, LU, LY, MA, MD, ME, MG, MK, MN, MW, MX, MY, MZ, NA, NG, NI, NO, NZ, OM, PA, PE, PG, PH, PL, PT, QA, RO, RS, RU, RW, SA, SC, SD, SE, SG, SK, SL, SM, ST, SV, SY, TH, TJ, TM, TN, TR, TT, TZ, UA, UG, US, UZ, VC, VN, ZA, ZM, ZW.

(84) Designated States *(unless otherwise indicated, for every kind of regional protection available)*: ARIPO (BW, GH, GM, KE, LR, LS, MW, MZ, NA, RW, SD, SL, SZ, TZ, UG, ZM, ZW), Eurasian (AM, AZ, BY, KG, KZ, RU, TJ, TM), European (AL, AT, BE, BG, CH, CY, CZ, DE, DK, EE, ES, FI, FR, GB, GR, HR, HU, IE, IS, IT, LT, LU, LV, MC, MK, MT, NL, NO, PL, PT, RO, RS, SE, SI, SK, SM, TR), OAPI (BF, BJ, CF, CG, CI, CM, GA, GN, GQ, GW, KM, ML, MR, NE, SN, TD, TG).

Declarations under Rule 4.17:

— *as to applicant's entitlement to apply for and be granted a patent (Rule 4.17(ii))*

[Continued on next page]

(54) Title: FLOW-INDUCED NOISE SOURCE IDENTIFICATION

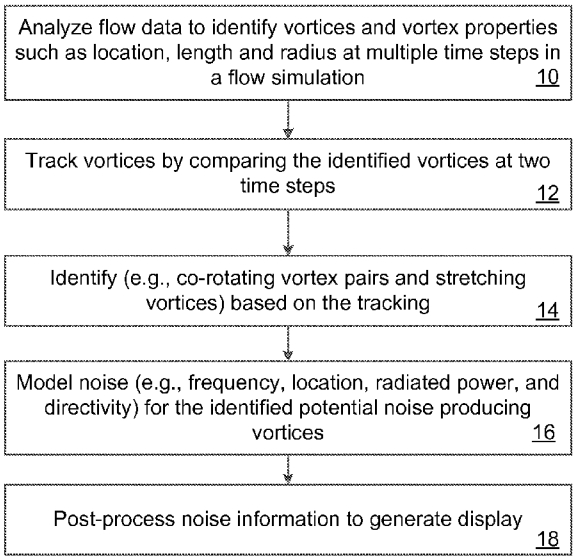

FIG. 1A

(57) Abstract: A system and method for automatically detecting and tracking time and space variations of flow structures in order to locate and characterize the flow structures which produce noise and to quantify the corresponding acoustic radiation properties. A system and method for automatically detecting and tracking time and space variations of flow structures in order to locate and characterize the flow structures which produce noise and to quantify the corresponding acoustic radiation properties is described herein.

WO 2014/137750 A1

— *as to the applicant's entitlement to claim the priority of the earlier application (Rule 4.17(iii))*

Published:

— *with international search report (Art. 21(3))*

FLOW-INDUCED NOISE SOURCE IDENTIFICATION

CLAIM OF PRIORITY

This application claims priority under 35 USC §119(e) to U.S. Provisional Patent Application Serial No. 61/773,360, filed on March 6, 2013 and entitled "FLOW-INDUCED NOISE SOURCE IDENTIFICATION," and U.S. Non-Provisional Patent Application Serial No. 14/069,691, filed on November 1, 2013, the entire contents of which are hereby incorporated by reference.

TECHNICAL FIELD

A system and method for automatically detecting and tracking time and space variations of flow structures in order to locate and characterize the flow structures which produce noise and to quantify the corresponding acoustic radiation properties is described herein.

BACKGROUND

In our society, acoustic comfort is taking a growing importance and a significant engineering time is spent on finding and developing noise reduction solutions. A major source of annoyance is related to flow-induced noise mechanisms such as jets, airframe, trains, rotating geometries and duct systems noise. Often expertise, intuition, and trial-and-error approach is used to identify which parts of a system should be worked on and optimized to reduce noise generation. In some additional examples, some experimental methods such as beam-forming, acoustic holography and two points correlation methods are productively used but require physical prototyping and wind-tunnel testing which are both time consuming and expensive. As another example, Computational AeroAcoustics (CAA) simulations provide flow field information to provide valuable insight on the flow topology.

SUMMARY

A method and system for tracking vortices and systems of vortices likely to radiate noise to the far-field is described herein. The methods described herein can also be used to capture transient and statistical properties of turbulent flow coherent structures.

In general, one aspect of the subject matter described in this specification can be embodied in methods that include the actions of simulating activity of a fluid in a volume, the activity of the fluid in the volume being simulated so as to model movement of elements within the volume. The method also includes, at a first time in the fluid flow simulation, identifying a first set of vortices in a transient and turbulent flow modeled by the fluid flow. The method also includes, at a second time in the fluid flow simulation that is subsequent to the first time, identifying a second set of vortices in the transient and turbulent flow. The method also includes, tracking changes in the vortices by comparing the first set of discrete vortices and the second set of discrete vortices, and identifying one or more potential sound generating vortex structures based on the tracking. Other embodiments of this aspect include corresponding computer systems, apparatus, and computer programs recorded on one or more computer storage devices, each configured to perform the actions of the methods. A system of one or more computers can be configured to perform particular operations or actions by virtue of having software, firmware, hardware, or a combination of them installed on the system that in operation causes or cause the system to perform the actions. One or more computer programs can be configured to perform particular operations or actions by virtue of including instructions that, when executed by data processing apparatus, cause the apparatus to perform the actions.

In general, one aspect of the subject matter described in this specification can be embodied in methods that include the actions of simulating activity of a fluid in a volume to generate flow data, the activity of the fluid in the volume being simulated so as to model movement of elements within the volume. The method also includes identifying one or more potential sound generating vortex structures based on changes in vortices between a first time in the fluid flow simulation and a second time in the fluid flow simulation and identifying one or more regions on a surface that generate the sound generating vortex structures based at least in part on the identified one or more potential sound generating vortex structures and the generated flow data.

The foregoing and other embodiments can each optionally include one or more of the following features, alone or in combination.

Tracking changes in the vortices can include executing a tracking algorithm that identifies a displacement of each vortex in the first and second sets of vortices between the first time and the second time.

Identifying the first and second sets of vortices can include identifying the first and second sets of vortices based on one or more of instantaneous pressure, vorticity, Q-criterion, and $\lambda 2$ criterion.

Identifying the one or more potential sound generating vortex structures can include identifying co-rotating vortex pairs based on the position and displacement of vortices in the first and second sets of vortices between the first time and the second time.

The method can also include for each identified co-rotating vortex pair determining an equivalent quadropole-like source, determining a corresponding acoustic radiation, and estimating the quadrupole-based far-field noise.

Identifying the one or more potential sound generating vortex structures can include identifying vortices undergoing stretching between the first time and the second time.

Simulating activity of the fluid in the volume can include performing interaction operations on the state vectors, the interaction operations modeling interactions between elements of different momentum states according to a model and performing first move operations of the set of state vectors to reflect movement of elements to new voxels in the volume according to the model.

Identifying the first set of vortices can include identifying a first set of vortex centerlines with each centerline corresponding to an associated vortex in the first set of vortices and identifying the second set of vortices can include identifying a second set of vortex centerlines with each centerline corresponding to an associated vortex in the second set of vortices.

Identifying the first set of vortex centerlines can include identifying a plurality of self-contained isosurfaces associated with the vortices in the first set of vortices, the identified isosurfaces having $\lambda 2$ values that are less than a threshold, performing a triangulation calculation to determine the centerline from the self-contained isosurfaces. Identifying the second set of vortex centerlines can include identifying a plurality of self-contained isosurfaces associated with the vortices in the second set of vortices, the identified isosurfaces having $\lambda 2$ values that are less than a threshold and performing a triangulation calculation to determine the centerlines from the self-contained isosurfaces.

Tracking changes in the vortices can include tracking the location and movement of the vortices.

The method can also include predicting sound generated by the identified one or more potential sound generating vortex structures.

Predicting the sound generated by the identified one or more potential sound generating vortex structures can include predicting the frequency, amplitude, intensity, power and location of the sound.

Predicting the sound generated by the identified one or more potential sound generating vortex structures can include predicting the directivity of the sound.

The method can also include filtering the predicted sound based on frequency.

The method can also include filtering the predicted sound based on directivity.

The method can also include generating a density map of the predicted sound from the identified noise producing vortex structures.

The method can also include generating an acoustic power map of the predicted sound from the identified noise producing vortex structures.

The method can also include identifying one or more regions on a surface that generate the sound generating vortex structures based at least in part on the identified one or more potential sound generating vortex structures and the simulated activity of the fluid in the volume.

The method can also include performing a geometry optimization process based on the identified one or more regions to generate a modified surface geometry.

Identifying the one or more potential sound generating vortex structures can include at the first time in the fluid flow simulation, identifying a first set of vortices in a transient and turbulent flow modeled by the fluid flow, at the second time in the fluid flow simulation that is subsequent to the first time, identifying a second set of vortices in the transient and turbulent flow, tracking changes in the vortices by comparing the first set of discrete vortices and the second set of discrete vortices, and identifying the one or more potential sound generating vortex structures based on the tracking.

Brief Description of the Figures

FIG. 1A shows a flow chart of a process for flow-induced noise identification.

FIG. 1B shows a flow chart of a process for flow-induced noise identification.

FIG. 1C shows a flow chart of a process for flow-induced noise identification.

FIG. 2A shows a schematic representation of a co-rotating vortices (CRV) system.

FIG. 2B shows a CRV system with different strength circulations.

FIG. 3 shows a schematic representation of a merging process for a co-rotating vortices system.

FIG. 4 shows a CRV simulation domain.

FIGS. 5A and 5B show fluid plane dB-maps for the time-evolution of two vortices.

FIGS. 5C and 5D show instantaneous frequency and the strength of the noise radiated by the vorticity fields show in FIGS. 5A and 5B.

FIG. 6 shows an exemplary reconstructed radiated acoustic field.

FIG. 7 shows an exemplary simulation of flow and acoustic fields corresponding to four points in time.

FIGS. 8A and 8B show the mean streamwise velocity component along the jet axis and streamwise velocity profile at 3mm upstream of the nozzle exit, respectively.

FIG. 9. shows the instantaneous vorticity field at various locations and planes.

FIG. 10A and 10B show a graph of instantaneous pressure fluctuations and a OASPL directivity plot, respectively.

FIGS. 11 and 12 show a plot of reconstructed centerlines and error spheres, respectively.

FIGS. 13 and 14 show a distribution of the vortices projected on the (x,y) plane and a distribution of vortex length along the x-axis, respectively.

FIG. 15 shows an example of reconstructed centerlines.

FIG. 16 shows an example graph of mean convection velocity along the x-axis.

FIG. 17 shows an example of reconstructed centerlines colored by stretching.

FIG. 18 shows an example graph of mean stretching per frame along the x-axis.

FIGS. 19A – 19D show exemplary simulation results including a density of noise sources.

FIG. 20 shows exemplary simulation results.

FIGS. 21A and 21B show two exemplary two jet nozzle designs.

FIGS. 22A and 22B show simulated spatial distributions of vortices for the nozzle designs of FIG. 21A and 21B.

FIG. 23 shows a simulated distribution of the noise sources for the nozzle designs of FIG. 21A and 21B at different bandwidths.

FIG. 24 shows a simulated total amount of noise sources detected for the nozzle designs of FIG. 21A and 21B.

FIGS. 25A and 25B show two exemplary car mirror designs.

FIGS. 26-32 show simulation results for the mirror designs of FIGS. 25A and 25B.

FIG. 33A and 33B show an exemplary baseline mirror and a Trailing Edge (TE) Extension mirror.

FIGS. 34-36 show simulation results for the mirror designs of FIGS. 33A and 33B.

FIGA. 37A and 37B show an exemplary geometry of HVAC system with ducts, vents and dashboard.

FIG. 38A and 38B show modifications of the ducts geometry.

FIG. 39A and 39B show modifications of the ducts geometry.

FIGS. 40-42B show simulation results.

Description

A Flow-Induced Noise Identification Method (FINSIM) is described herein. Coherent vortex structures in flows are closely related to the flow-induced noise generation mechanisms and it is assumed that by characterizing the time and spatial evolutions of relevant vortices, the physical sources that are responsible for generating the noise can be identified. More particularly, a method and system for identifying and tracking vortices and systems of vortices likely to radiate noise to the far-field is described herein. In case of thermal configurations, FINSIM can also be used to analyze space and time variations of the temperature field (or any relevant passive or active scalar field) to estimate the acoustics radiation of entropy sources.

The systems and methods described herein identify noise produced by the vortex motions (e.g., Co-Rotating Vortex systems - CRV) and vortex stretching. For example, the system identifies:

1. Each relevant vortex pair as discrete CRV systems and determines the equivalent quadrupole-like sources and corresponding acoustic radiation (e.g., the transient flow field is used to track the CRV motion and reconstruct the radiated field according to Powell's theory);

2. Stretching rate of each vortex detected in the flow and corresponding dipole-like acoustic radiation; and/or

3. Entropy sources and corresponding monopole-like acoustic radiation.

By analyzing the motion of the entire flow field of vortices, the complete far-field noise can be estimated and properties of the physical noise sources can be analyzed.

Overview

FIG. 1A shows a flow chart of a process for flow-induced noise identification. The system receives transient flow data from a fluid flow simulation from computational fluid dynamics solvers based, for instance on Navier-Stokes and Lattice Boltzmann. Such simulation data provides the time and space dependent volumetric information used to identify vortices.

The method includes analyzing flow data to identify the vortices and vortex properties such as location length and radius and circulation at multiple time steps in the flow simulation (10). As described in more detail below, for each time frame, the system identifies multiple vortices with each vortex being represented by a set of connected points referred to herein as a centerline of the vortex. The centerlines for each vortex and the location of the vortices can be generated using various techniques. For example, in a three-dimensional simulation, a λ_2 criterion (e.g., a criterion used to identify a vortex region as a region where the second eigenvalue λ_2 ($\lambda_1 \geq \lambda_2 \geq \lambda_3$) of the symmetric tensor ($\Omega_2 + S_2$) is negative at every point inside the vortex core) can be used to identify regions in the simulated system likely to include a vortex. The regions identified as being likely to include a vortex collectively can be represented as an isosurface that includes regions having λ_2 values that fall below a threshold manually imposed or automatically determined by the method. Thus, the identified isosurface will include multiple regions within the simulation space and will contain all of the vortices satisfying the threshold condition. Further computation of the isosurface can be completed to identify self-contained portions of the isosurface associated with distinct vortices. For example, a flooding algorithm can separate non-touching clumps of voxels (such that each clump corresponds to one vortex / one group of touching vortices) and subsequently an algorithm can split big clumps of voxels in smaller clumps such that each clump represents a single vortex (the subdivision process can be repeated more than once). In some examples, clumps of voxels containing less than a threshold number of voxels, or having a maximum circulation less than a threshold number, can be removed (e.g., to remove negligible vortices from consideration). Once such self-contained

isosurfaces have been identified, an algorithm can be used to triangulate or otherwise determine a centerline for each of the identified vortices. As described in more detail below, other quantities such as vorticity and/or a Q-criterion can be used to identify the vortices.

Once the set of vortices in the system has been identified for at least two time frames in the fluid flow simulation, the method includes a spatial tracking of the vortices by comparing the identified vortices at two different time steps (12). More particularly, an algorithm matches - if possible - each of the vortices at the first time step with an associated vortex at the second time step based on their centerline representations. In addition, the algorithm determines whether a particular vortex in the second time frame is an instantiation of a previously identified vortex, a new vortex, a split of the vortices into multiple new vortices, or a merge of multiple vortices in a new single vortex. By tracking the motion of each of the vortices, information about the size, velocity, intensity, stretching, direction of movement and any dynamic information regarding each vortex is generated.

Using the tracking information, the system identifies simple or complex systems of vortices that are likely candidates for noise producing vortices (14). More particularly, co-rotating systems or vortices with a high stretching rate are more likely than other vortices to produce noise. As such, based on the tracking information vortices or systems of vortices satisfying these characteristics (e.g., co-rotating vortices and vortices undergoing stretching by getting longer or shorter or being twisted) can be identified based on the size, velocity and direction of movement information.

After the vortices and systems of vortices have been identified, the system models the noise produced by the vortices (16). The noise modeling includes a reconstruction of the frequency, amplitude, location, directivity, and radiated power for each source and for the overall system composed of all individual sources. In case of co-rotating vortices, all the previous information is reconstructed based on a theory of the vortex sound derived from a generalization of Powell's theory. This theory makes the link between the vortex dynamics (e.g., rotation speed, growth rate, and/or relative motion) and the noise generation. In case of stretching vortices, the tracking algorithm coupled to a dipole-like noise modeling derived from Powell's theory gives access to the stretching noise contribution. This contribution is related to the evolution of the shape, length, intensity, circulation, and the deformation rate of the vortex structures.

The system also performs post-processing operations on the determined noise information to extract and display useful features of the information to the operator of the system (18). For example, post-processing of the data can be used to generate a density map of the noise producing structures. For example, the noise data from multiple different time frames can be summed to generate a density map that shows the frequency of a noise producing structure based on the noise produced by the co-rotating vortices and the stretching vortices. In another example, post-processing can be used to identify places with a high count of noise producing structures. In another example, the noise data from multiple different time frames can be summed up to generate a time-averaged radiated acoustic power map based on the noise produced by the co-rotating vortices and the stretching vortices. In another example, post-processing can be used to filter the noise producing structures by a direction to see a density and count of the noise producing structures, but only for the noise directed in a particular direction. In another example, the data can be post-processed based on a frequency such that only certain frequencies of noise are displayed to the user. In another example, information on the sources can be coupled to the flow data to identify and locate regions of the surrounding geometry responsible for the generation of the noise (such as steps, gaps, and/or sharp edges).

Overview of Powell's theory of vortex sound

As noted above, one method to determine sound generated in a system can be based on an application of Powell's Theory of Vortex Sound. In free flows, the flow-induced sound is considered to be generated by the motion of vortices. There are no momentum changes, since no solid surfaces are present, which implies that when a change in vorticity occurs somewhere in the flow, the opposite change occurs somewhere else. Each vortex experiences a change in strength and shape, which in both case, generate a dipole-like radiation. The following general expression for the far-field acoustics density fluctuations due to vortex motion can then be derived:

$$\rho'(\vec{x},t) \approx -\frac{\rho_\infty}{4\pi c^4 x}\frac{(x_i x_j)}{x}\frac{\partial^2}{\partial t^2}\int_V y_j(\vec{\omega}\times\vec{u})_i dV(\vec{y}) \tag{1a}$$

with y_j the projection of the integration vector $\vec{y}$ on $\vec{e_j}$, $\vec{x}$ the observer position vector, $\vec{\omega}$ the vorticity vector and $\vec{u}$ the velocity vector. $dV(\vec{y})$ is the elementary volume of fluid. ρ_∞ is the mean density and c is the speed of sound. A discretization of the volume of integration V in

terms of vortex corelines elements is used and a new expression for far-field density fluctuations is derived from Eq. 1a:

$$\rho'(\vec{x},t) \approx -\frac{\rho_\infty}{4\pi c^4 x}\frac{(x_i x_j)}{x^2}\frac{\partial^2}{\partial t^2}\sum_{k=vortex}(y_k)_j\left(\vec{\Gamma}_k \times \vec{u}_k\right)_i \Delta l_k \tag{1b}$$

with k representing one sub-element of one unique discretized vortex coreline. A system of two co-rotating vortices 30, 32 distant by $2y$ with the same circulation Γ (represented by arrows 34 and 36, respectively) as represented in FIG. 2A is now considered. Such a system induces the rotation of the vortices around an axis O *(38)* at the angular velocity $\Omega_s = \Gamma/(4\pi y^2)$ for which Γ and y are constants. By using this angular velocity in Eq. 1b, the density fluctuations are now given by:

$$\rho'(\vec{x},t) \approx -\rho_\infty 4\sqrt{\pi}\sqrt{\frac{\Delta l}{R}}\cos\left(2(\vec{x},\vec{e_1}) - 2\Omega_s t^* + \frac{\pi}{4}\right)\left(\frac{\Omega_s y}{2c}\right)^{\frac{7}{2}} \tag{2}$$

with Δl the length of the vortex coreline element. We suppose $\Delta l \ll \lambda$ so that time delay of the acoustic waves is neglected, with λ the acoustic wavelength. The unit vectors used in Eq. 2 are described, for example, in FIG. 2A which provides a schematic representation of a co-rotating vortices (CRV) system. Consequently, the radiated sound power corresponding to this CRV system is:

$$P_{tot} = \oiint \frac{\langle \rho'^2(\vec{x},t)\rangle c^3}{\rho_\infty} d^2S = \frac{\rho_\infty \Delta l \pi^2 \Omega_s^7 y^7}{8c^4} \tag{3}$$

Powell's theory neglects viscous effects (discussed below) and as a consequence a perpetual motion of the CRV occurs. The equivalent acoustic system is a rotating quadrupole composed of four constant pressure poles rotating around an axis.

Sound is also generated by the change in strength of vortices in the flow. For example, Aeolian tones are produced by the stretching of vortex rings and the radiated noise is equivalent to dipole radiation. However, such changes in strength do not occur isolated in the flow and an opposite stretching is likely to be found at a delayed period in time, resulting in a shedding. Consequently,

an oscillating quadrupole-like noise source is to be found. Powell also developed the theory for the dipole-like radiation. The corresponding equation for fluctuating velocity is:

$$\vec{u}\,(\vec{x}) = -\frac{\vec{x}}{4\pi x^2 c^2}\int \mathcal{L}'_x dV(\vec{y}) \tag{4}$$

with $\vec{\mathcal{L}} = \vec{\omega} \times \vec{u}$ then Lamb vector and $\mathcal{L}'_x = \frac{\partial(\vec{\mathcal{L}}|\vec{e_x})}{\partial t}$. In vortex stretching, the sound radiation occurs because the acceleration of a vortex element in a direction normal to its axis causes a local fluctuating dipole-like flow (obtained through space integration of the time derivative of the Lamb vector).

Extensions of Powell's theory

In Powell's theory, vortices are represented through their circulations and locations centered on a spinning axis. In order to take into account for the variation in both size and circulation of vortices, the Scully vortex model is used for the rotational velocity:

$$V_\theta(r) = -\frac{\Gamma r}{2\pi(r_c{}^2 + r^2)} \tag{5}$$

The difference in strength of the two vortices has an impact on the rotating system. Considering two vortices (e.g., vortices 50, 52 in FIG. 2B) with different circulations, according to the parameters defined in FIG. 2B, the angular velocity of the system is:

$$\Omega = \frac{\Gamma_1 + \Gamma_2}{2\pi b^2} \tag{6}$$

The position of the center of rotation is given by:

$$x_O = \frac{\Gamma_1 x_1 + \Gamma_2 x_2}{\Gamma_1 + \Gamma_2}, \qquad y_O = \frac{\Gamma_1 y_1 + \Gamma_2 y_2}{\Gamma_1 + \Gamma_2} \tag{7,8}$$

Starting from Eq. 1b and using the geometrical parameters of the system (FIG. 2B), the density perturbations and acoustics power become:

$$\rho'_{12}(\vec{x},t) \approx -\frac{\rho_\infty}{8\pi^2 c^4}\frac{1}{(R^2+Z^2)^{\frac{3}{2}}}R(2R\cos(2\theta-2\Omega_s t^*)+Z\cos(\theta-\Omega_s t^*))\Delta l\Omega_s^2\Gamma_1\Gamma_2 \quad (9)$$

$$P_{tot} = \frac{17\rho_\infty\Gamma_1^2\Gamma_2^2\Delta l^2\Omega_s^4}{240\pi^3 c^5} \quad (10)$$

with R, θ and Z the cylindrical coordinates of $\vec{x}$ in the frame of reference of the CRV system.

This assumes the shape of the vortices stays coherent (i.e. well approximated by a point model). If the ratio of the circulations is above a certain threshold, more complex viscous effects happen introducing noise generation through changes in size of the low circulation vortex. FIG. 2A shows an exemplary schematic representation of a co-rotating vortices (CRV) system and FIG. 2B shows an exemplary schematic representation of a co-rotating vortices system with different strength circulations.

When viscous effects are taken into account, more complex mechanisms are involved and the CRV vortex pair eventually merges. The merging process consists of four stages:

- First diffusive stage,
- Convective stage,
- Second diffusive stage,
- Final diffusive stage.

The first diffusive stage corresponds to the diffusion of each vortex due to its rotation and the viscosity of the fluid, which causes an increase of their core radii following a square root law $r_c(t) = r_c(0) + c\sqrt{\nu(t-t_0)}$. During this stage, the quadrupole analogy of Powell can be successfully applied. The convective stage starts when the core radius reaches a critical value such as $r_{c\,critical} = 0.290b_0$ with $b_0 = 2y_0$ the initial distance between the two vortices. The coefficient in front of b0 depends on the precise setup conditions. The duration t_c of the convective stage in case of laminar vortices is known from experiments: $t_c = 8.1 * (b_0^2/\Gamma_0)$. The distance between the vortices decreases during this stage and diffusion plays only a minor role. Also during this stage, the rotation speed increases, creating a non-symmetric vorticity field giving birth to vorticity filaments. The second diffusive stage corresponds to the period necessary for the vortices to merge (b=0), and the final diffusive stage is the diffusion of the

resulting single post-merge vortex. The four stages are illustrated in FIG. 3, obtained from LBM simulations of the CRV system described herein. FIG. 3 shows the Instantaneous vorticity field Ω [s^(-1)] obtained from a LBM CRV simulation at (a) first diffusive step, (b)convective step, (c) second diffusive step, (d) final diffusive step.

Noise Source Identification

The flow-induced noise identification method (FINSIM) approach described herein identifies and tracks the vortex structures responsible for sound generation in arbitrarily complicated flows of real industrial cases. The vortex structures of interest are co-rotating vortex (CRV) pairs and vortices undergoing stretching (e.g., at a non-uniform rate). For the CRV sources, FINSIM identifies each relevant vortex pair as a discrete CRV system and determine the equivalent quadrupole-like sources and corresponding acoustic radiation. By studying the motion of the entire flow field of vortices, the complete quadrupole-based far-field noise can be estimated, and properties of the physical noise sources can be analyzed. The proposed tracking scheme is valid during the first diffusive stage and the beginning of the convective stage of the CRV motions, which are believed to be the most important mechanisms for noise generation.

Referring to FIG. 1B, a flow diagram for the flow-induced noise identification method (FINSIM) approach is shown. At a high level, the FINSIM approach includes vortex detection 102, vortex tracking 114, and noise modeling 128/130 to generate noise properties 132.

The vortex detection 102 portion of the FINSIM approach is used for the identification of vortices. The identification of vortices can be based on instantaneous pressure, vorticity, Q-criterion, λ2-criterion or other methods able to identify discrete vortices in a transient and turbulent flow. In two dimensions, vortices can be extracted based on the vorticity. For 3-D cases, the use of the λ2-criterion is likely more suitable.

More particularly, as shown in FIG. 1C, the vortex detection process 102 receives a measurement file 100 from a flow simulator (150). The measurement file includes information about the flow of particles in each voxel (or in a subset of voxels for an identified region) in the system including pressure and velocity vector minimum. The measurement file includes one or more frames (e.g., separate time steps in the simulation) of flow data. Based on the flow data, the system computes λ_2 and vorticity vector for each voxel for each frame (152). These values

can be used to locate a vortex. For example, a low value of λ_2 is likely to be close to the centerline of a vortex. The λ_2 and vorticity vector are then used to generate vortex clumps of voxels (e.g., an isosurface) with each clump corresponding to one vortex / one group of touching vortices (154). To generate the clumps of voxels, the system compares the values for the λ_2 and vorticity vectors to pre-determined thresholds to select a subset of voxels having λ_2 and vorticity vectors with values in a pre-determined range. The initial clumps of voxels can include overlapping vortices, so the system refines vortex clumps to separate each group of touching vortices into single vortices (156). In order to remove small vortices, (e.g., vortices less than a threshold size), the system filters clumps based on size (158). For remaining clumps of voxels, the system generates a centerline for each clump of voxels (160). The centerline information includes various vortex properties 104 such as location 106 and length and radius 108.

The vortex tracking portion 114 of the FINSIM approach identifies the displacement of each vortex. In this portion, the parameters of all vortices (location, radius, circulation, etc) at discrete time t_i and t_{i+1} are computed and a tracking algorithm identifies the displacement of each vortex between t_i and t_{i+1}. More particularly, a tracking algorithm receives centerline data from a current frame of the simulation 110 and centerline data from a previous frame of the simulation 112. Based on these two sets of centerline data, the tracking algorithm generates vortex dynamic information 116. This includes trajectory information 118, convection velocity 120, and information about stretching/deformation of vortices 122. Based on the vortex dynamic information 116 the tracking algorithm can output tracking data associated with co-rotating vortex pairs 124 and stretching data 130 associated with vortices undergoing stretching. Identifying the co-rotating vortex pairs can include, for example, analyzing the vortex system motion. The identification of each CRV system is based on the calculation of the position and displacement of each vortex and the determination of their closest neighbors. The vortex and their neighbors are then considered as discrete CRV systems. The number of candidate CRV systems is reduced by discarding systems which inter-vortex distance is above a distance threshold. The self-rotation information of the CRV system is extracted from its dynamics and used for modeling.

Identifying the stretching vortices can include, for example, computing the growth rate of individual structures length or circulation (information known from the structure identification

procedure). From the change in length or strength of the vortices, stretching vortices are detected.

The noise modeling portion(s) 128, 130 of the FINSIM approach derive the noise generated by the identified vortices. More particularly for each CRV, based on its dynamics, the resulting generated noise is derived according to the extended Powell's theory. Noise generation due to vortex stretching is also derived. The noise modeling generates a set of noise properties for the system (e.g., a summation or compilation of the noise properties for each noise producing vortex in the system). The noise properties can include the frequency 134, location 136, directivity 138, and radiated power 140 for vortices in the system. The noise properties can be identified and associated with locations in the simulated system. For example, the noise properties for each voxel in the system can be determined. The frequency information 134 is important because some frequencies of sound are more likely to cause disturbance while other frequencies may be outside of the spectrum that can be perceived by human ears. The location information 136 can be useful to identify places within the system that generate noise. This information can be used to trace back to noise producing structures in the physical design of the object being simulated. The physical location in the design responsible for the inducing noise vortices can be determined, for example, by implementing a reverse problem. Knowing the location of a noise source in the flow, it is possible to identify where the vortices responsible for sound were originally generated using, for example, the mean flow streamlines, the vortex trajectory or a reverse particle-tracking algorithm. The location information can be displayed as a graph with the voxels having noise producing vortices identified on the graph. The directivity information 138 for vortices can also be important. For example, if a side mirror on a car is generating noise but the noise is directed away from the car rather than toward the window the impact of the noise to the comfort of the individuals in the car may be reduced and therefore the noise may be less of a concern. Finally, the radiated power or amplitude of the noise 140 is important because the tolerance for certain levels of noise may make changes to the system unnecessary if the level of noise falls below a threshold.

While not shown in FIG. 1B, post processing of the noise data can be beneficial to provide understandable and useful information to a user. For example, based on the results generated for the predicted flow and radiated noise useful metrics, displays, and information can be presented to the user. These can include information and statistics about vortex locations and

convection speeds, characteristic vortex lifetime, vortex stretching behavior, instantaneous radiated frequencies, noise source locations and strength, frequency-dependent intensity maps, etc.

In one example, post processing can be used to generate a graph of the vortex locations and convection speeds. This map provides an indication of the convection speed by coloring or otherwise providing a visual indicator of the convection speed for each voxel. Locations for which there are no vortices present will be similarly colored to indicate the absence of vortices (e.g., because there will be no associated convection speed or the convection speed will be below a threshold). In some examples, the map of vortex location convection speed is displayed for a single time point while in other examples a time evolution of multiple time frames is provided.

In another example, post processing can be used to generate a graph of the vortex locations by providing a visual representation of the centerline locations. For example, the centerlines can be displayed on the representation of the system by an appropriate visual indicator within the voxel. Since a centerline will span multiple voxels, the centerlines for voxels will be displayed by providing the appropriate indicator in each of the voxels. Additionally, the strength or the amplitude of the noise radiated by the centerline can be visually indicated. For example, if the centerline is represented by a line at the appropriate location(s), the width or coloring of the line can provide information about the amplitude of the sound produced by the vortex. Such information can be displayed for a single time step in a simulation or as a time-based evolution spanning multiple time steps.

In another example, post processing can be used to generate a graph of the frequency of sounds produced within a system. For example, a graph of the noise source density (e.g., the number of vortices within the system) versus the frequency of sound produced by the vortex can be generated. In another example, a graph of the radiated acoustic power (e.g., the time-averaged acoustic power generated by the various system of vortices) versus the frequency of sound produced by the vortex can be generated. In some examples, multiple different designs are simulated and a comparison of the generated sound frequencies can be provided (e.g., a graph that includes information for both designs).

In another example, post processing can be used to generate a graph of the vortex locations and strength. This map provides an indication of the vortex strength by coloring or otherwise providing a visual indicator of the convection speed for each voxel. Locations for

which there are no vortices present will be similarly colored to indicate the absence of vortices (e.g., because the strength will be below a threshold).

In another example, post processing can be used to generate a graph of characteristic vortex lifetime. For example, a graph of the distribution of vortices according to the total travelled distance can be generated. Turbulence in many designs can be an issue and the lifespan of coherent structures must be reduced to avoid mechanical fatigue or object indirect interactions. An appropriate design can be chosen by minimizing the travelling distance of vortices.

In another example, post processing can be used to generate a graph of vortex stretching behavior. For example, a plot of the stretching rate of vortices along a specific direction of the simulated object can be generated. In some designs, the turbulence in the flow, i.e. the vortices, must decay in intensity or size as fast as possible, and an efficient design can be determined by looking at the stretching rate distribution.

In another example, post processing can be used to generate a graph of instantaneous radiated frequencies. For example, a spatial map of noise sources colored by frequency can be generated, presented as a time animation. In some designs, the noise generated in the flow can reach unauthorized level, corresponding to peaks in the SPL graph of a far-field probe. A map of the sources colored by frequency will help identify regions of the flow responsible for this specific tone and it will provide insight on the life cycle of the noise inducing vortices responsible for such levels through a time animation of the sources motion.

In another example, post processing can be used to generate a frequency-dependent intensity maps. For example, a graph can be generated to provide an indication of the vortex strength by coloring or otherwise providing a visual indicator of the convection speed for each voxel. The information on this graph can be filtered to display a user-selected range of frequencies. For example, the user may desire to display only frequencies that are detectable by the human ear or only high frequencies that may be perceived to be more disruptive to an individual's comfort. Filtering by frequency in the associated voxel based graph allows the user to focus attention on locations within the system that are generating the highest amount of noise within a frequency range of interest.

In another example, post-processing can be used to generate the graph of power over a range of frequency of interest. For example, the SPL graph of the mean power during the

simulation time of all sources within a defined region can be generated. For some objects, the flow-induced noise can originate from several locations in space. In the far-field, it can be difficult to pinpoint which quantity of acoustic power comes from which region, and computing this information helps a better design process by prioritizing parts of the object that need modifications for noise reduction.

In another example, post-processing can be used to generate the directivity of power for a specific region. For example, the distribution of time-averaged acoustic power over a sphere centered on a specific region of interest can be generated. When designs are compared, not only the total amount of power radiated is important but also its directivity. Depending on the direction, the radiated acoustic power can be of interest, i.e. a direction where the noise needs to be reduced, or it can be negligible, i.e. a direction where the noise has no importance.

In another example, post-processing can be used to generate the reconstruction of acoustic signals at various points in space. For example, the pressure acoustic field on any surface can be visualized or used to quantify the amount of acoustic power transmitted. In the flow region, the acoustic pressure field is not directly available as it can be hidden in the hydrodynamic pressure field fluctuations. Filtering is difficult and can be contaminated by numerical noise. Using the modeling of noise sources, the acoustic filtering can be performed with the reconstruction of the acoustic pressure field at any point of interest in the flow region.

In another example, post-processing can be used to generate a surface map of the noise source origin. For example, the surface of the object can be locally colored by the number of flow induced noise sources which originated from the location of interest. In some designs, specific regions of the surface responsible for noise generation need to be highlighted before being corrected. By modifying the highlighted pieces of surface, the noise sources can be decreased in intensity and the design improved.

Lattice Boltzmann Method (LBM)

As noted herein, various types of flow simulations can be used to generate the flow information used to identify and track vortices. One such flow simulation is based on the Lattice Boltzmann Method. A CFD/CAA code is used to compute unsteady flow physics. The code is

based on the Lattice Boltzmann Method (LBM). Lattice based methods were proposed as an alternative numerical method to traditional Computational Fluid Dynamics (CFD). Unlike conventional methods based on discretizing the macroscopic continuum equations, LBM starts from "mesoscopic" kinetic equations, *i.e.* the Boltzmann equation, to predict macroscopic fluid dynamics. The lattice Boltzmann equation has the following form:

$$f_i(\vec{x} + \vec{c_i}\Delta t, t + \Delta t) - f_i(\vec{x}, t) = C_i(\vec{x}, t) \tag{11}$$

where f_i is the particle distribution function moving in the i^{th} direction, according to a finite set of the discrete velocity vectors $\{c_i: i=0,..b\}$, $c_i\Delta t$ and Δt are respectively space and time increments. For convenience, we choose the convention $\Delta t=1$ in the following discussions. For the collision term on the right hand side of Equation (11) the simplest and most common implementation is the Bhatnagar-Gross-Krook (BGK) form:

$$C_i(\vec{x}, t) = -\frac{1}{\tau}[f_i(\vec{x}, t) - f_i^{eq}(\vec{x}, t)] \tag{12}$$

Here τ is the relaxation time parameter, and f_i^{eq} is the local equilibrium distribution function, which follows the Maxwell-Boltzmann form. The basic hydrodynamic quantities, such as fluid density ρ and velocity u, are obtained through moment summations:

$$\rho(\vec{x}, t) = \sum_i f_i(\vec{x}, t), \qquad \rho\vec{u}(\vec{x}, t) = \sum_i \vec{c_i} f_i(\vec{x}, t) \tag{13,14}$$

In the low frequency and long-wave-length limit, for a suitable choice of the set of discrete velocity vectors, the transient compressible Navier-Stokes equations are recovered as shown by Chapman-Enskog expansion. The resulting equation of state obeys the ideal gas law, and the kinematic viscosity of the fluid v is related to the relaxation time parameter τ and the temperature T:

$$\nu = \left(\tau - \frac{1}{2}\right) T \tag{15}$$

The combination of Equations (11-15) forms the usual LBM scheme for fluid dynamics. It is solved on a grid composed of cubic volumetric elements called voxels, and a Variable Resolution (VR) strategy is allowed, where the grid size changes by a factor of two for adjacent resolution regions.

Co-Rotating Vortices (CRV)

A. Numerical setup

LBM Direct Numerical Simulation (DNS) are used to simulate a CRV system and two initial vortices are defined as an initial condition using Scully's model with a core radius r_c =8x10^{-4} m and a circulation $\Gamma = 4\pi r_c v_{max}$ with $v_{max} = 0.3$ m/s. The initial distance between the vortices is b_0=1.6x10^{-4} m and the Reynolds number Re based on v_{max} and r_c is Re=159. The simulation domain is a $2048r_c$ square 60 (FIG. 4). The simulation domain 60 is surrounded by a sponge zone 62 consisting in several layers of fluid with increasing viscosity and resolution in order to avoid acoustic reflection at the boundaries. The boundary conditions on the exterior edges of the sponge zone are pressure outlets with non reflective conditions and the characteristic pressure is p_0=101325 Pa. The smallest voxel size is $\Delta x = r_c/30$. The *a priori* estimated wavelength of the CRV radiation being $\lambda = 1000r_c$ the simulation domain and the measurement region are large enough to capture the radiated acoustic field. The simulation is performed until the merging process is over, that is to say for T=13.3x10^{-3} s corresponding to 300,000 time-steps.

B. CRV simulation results and analysis

FIG. 3 shows a schematic representation of a merging process for a co-rotating vortices system. In FIG. 3, the instantaneous vorticity fields are represented in FIG. 3 and it is seen that the four stages of the CRV are recovered. The predicted angular velocity from a kinematic

analysis is ω_0=208.3 Hz. The converged value obtained after a short initial transient of the simulation (t=0.3ms) is $\omega_{0\text{-}sim}$=208Hz +/- 3Hz, in very good agreement with the theoretical value. The simulation vortex core radius as a function of time shows a square law dependency with an expansion coefficient α=2.3. From Cerretelli and Williamson, the value is α=2.24 for Lamb Oseen vortices while α=1.9 is found experimentally, which compare reasonably well to the predicted value.

The complete time-evolution of the two vortices was analyzed to enable the desired quadrupole modeling, in particular the time-dependent characterization of the quadrupole noise sources. FIGS. 5A-5D show Vorticity isocontours (s^{-1}) and dB spatial map (dB) for co-rotating vortices with Re=159 with a) and b) are computed at t = 0.91ms. c) and d) are computed at t = 6.38ms. In FIGS. 5b and 5d, fluid plane dB-maps (i.e. images with voxels / areas colored by fluctuating pressure level) are shown highlighting the instantaneous frequency and the strength of the noise radiated by the vorticity fields plotted in FIGS. 5a and 5c, respectively. This representation shows the physical noise sources without any notion of directivity. It is observed that the frequency of the radiation is increasing with time as the two vortices get closer and closer and accelerate. The acoustic power is also increasing until the system collapses due to the merging process.

The entire reconstructed radiated acoustic field is shown in FIG. 6. The comparison between the acoustic field obtained directly with the LBM simulations (in gray scale) and the pressure wave extrema calculated with FINSIM (represented by lines 72, 74) are in a satisfying agreement, which provides a validation of the algorithm for the noise modeling step. While this is only a 2D example, it shows that the concept (of predicting sound generation via CRV tracking) works. More particularly, in FIG. 6, the black and white shows the filtered acoustic pressure field in the range [-0.5Pa,0.5Pa] between 200Hz and 1500Hz predicted from LBM and lines 72, 74 correspond to minimum and maximum pressure wave values calculated with FINSIM.

2-D Shear layer flow

A. Shear layer flow

In previous studies it is shown that the noise generated by the main structures of a shear layer has a quadrupolar nature and is related to a vortex pairing mechanism very similar to the isolated CRV system. Here a two-dimensional forced shear layer at its first harmonic frequency f_0=40 KHz. is simulated in order to demonstrate FINSIM on a relatively simple case for which the crucial noise source dynamics and resulting sound field are known.

The Shear Layer (SL) problem is characterized by three parameters: the thickness $\delta_w(0)$, the maximum velocity U_1 and the minimum velocity U_2. The inlet velocity profile is given by:

$$u(y) = \frac{U_1 + U_2}{2} + \frac{U_1 - U_2}{2}\tanh\left(\frac{2y}{\theta}\right) \tag{16}$$

with $\theta = \delta_w(0)$. In the case of the forced shear layer, a sinusoidal forcing component is added to θ such as $\theta = \delta_w(0)(1 + 0.8\sin(2\pi f_0 t))$. The corresponding Reynolds number is Re= 250 with $\delta_w(0) = 4.34\text{x}10^{-5}$m.

The simulation domain extends over $9600\delta_w(0)$ in the y-direction and over $8800\delta_w(0)$ along x. Sponge zones are again used to provide an anechoic condition. 2-D DNS simulations are performed over 80 cycles, i.e. 80 primary pairings. As shown in FIG. 7 for the forced SL, the flow is periodic, and the detection method is applied at four instants in time during one pairing period of two consecutive vortices generated in the SL. The time-dependent flow results are processed with FINSIM and the quadrupolar noise sources are recovered and can be explicitely associated to the pairing mechanism (FIG. 7). The main radiated frequency corresponding to the pairing frequency is also recovered showing a dependency on time and space. More particularly, FIG. 7 shows flow and acoustic fields corresponding to four points in time within one pairing period of the forced shear layer flow. From top to bottom: t=0 s; t=0.146 s; t=0.151 s; t=0.161 s. The graph on the left shows isocontours of vorticity in s-1, the graph in the middle shows instantaneous spatial dB-maps of noise sourcesand the graph on the right shows reconstructed acoustic field where lines 72 are pressure wave minima and lines 70 are pressure wave maxima.

3-D jet flow

A. Numerical setup

Jet flow is an important source of noise in numerous applications, from aerospace to heavy machinery. While the mechanisms of noise generation (turbulence generation and vortex-to-vortex interaction) have been extensively analyzed by many researchers, the influence of geometric design details on how and where exactly the noise is generated is not explicitly understood. Therefore jets provide a compelling example for noise source identification.

Simulations of a round jet are performed on the CMS000 configuration (see for example FIG. 11). A large 3-D transient flow data set is generated to aid in the development and validation of FINSIM including the extension to 3D. The characteristic length is D=50.8 mm corresponding to the nozzle diameter.

The jet Mach number is M=0.35 and Reynolds number Re=410,000. The resolution is Δx=1 mm and physical time t=0.1s of simulations are performed. Similarly to the previous 2-D cases, a sponge zone scheme surrounding the nozzle and the jet is used in order to avoid spurious reflections from the boundaries of the domain.

B. Flow and noise results

FIGS. 8A and 8B show the mean streamwise velocity component along the jet axis and streamwise velocity profile at 3mm upstream of the nozzle exit, respectively. In FIGS. 8A and 8B, the mean stream-wise velocity component is compared to experiments both along the jet axis, and the nozzle profile at 3 mm upstream of the exit. The predicted results are in good agreement with experiments. In particular, the boundary layer inside the nozzle is accurately predicted and the jet expansion, together with the potential core length are well recovered. Instantaneous snapshots of the vorticity field are represented in FIG. 9 showing the presence of a large number of vortices in the jet (FIG. 9. Shows the instantaneous vorticity field at various locations and planes), including structures present in the shear layers and induced by the turbulent mixing of the jet at the end of the potential core.

The acoustics radiation is captured within the same transient simulation and a snapshot showing the instantaneous pressure fluctuations is plotted in FIG. 10A with FIG. 10 showing Instantaneous pressure fluctuations in a x-aligned plane. A main source of noise is visible in this

figure, coming from the end of the potential core. The directivity of the overall sound level measured at microphones located 100D from the nozzle exit is shown in FIG. 10B with FIG. 10B showing OASPL directivity plot. The noise levels and the directivity dependence are well predicted and in particular the increase of the noise levels with increasing observation angle is obtained.

C. FINSIM Results

The source identification method previously presented is adapted to 3-D transient inputs and used to analyze the sources of noise of the 3-D jet simulation. First, the simulation measurement files are input to the vortex detection method, which returns vortex core centerlines and other geometrical information about each vortex such as radius, location, length, etc. From the vortex centerlines and radii (i.e. the average radius of the λ-2 isosurface), the vortex structures are reconstructed in simplified form as visualized in FIG. 11 (e.g., showing the reconstructed centerlines). A high density of vortices is observed in the shear layer close to the potential core where vortices are produced. Vortices are then convected downstream, with vortex density decreasing due to merging and dissipation. In order to assess the accuracy of the vortex reconstruction process (which generates a "skeleton" version of each vortex), an error is computed based on the averaged distance of the initial isosurface envelope to the reconstructed mesh of the vortex. The average distance is then normalized by the equivalent radius of the individual skeleton. FIG. 12 shows the results of this computation, where each vortex is represented as a sphere with a radius that corresponds to the size of the error. The numerical values of this error metric generally stay under 1.0, and though peak values up to 3.0 are observed, the error levels are thought to indicate an acceptable accuracy for the reconstruction process. The peak values actually correspond to complex intertwined structures that are not individually captured by the first step of the process. If a single isosurface represents several blended vortices at the same time, FINSIM treats it as one, trying to fit a single tube to a complex system of vortices.

Vortex tube information, obtained for all frames, allow us to perform statistics on the turbulence in the flow. FIG. 13 shows a distribution of the vortices projected on the (x,y) plane. In FIG. 13, each vortex location from each frame is orthogonally projected on a 100cellsx100cells grid centered on the jet axis, representing a total width of 3D. The fraction of

vortices whose projection falls inside each individual grid cell is represented by the color of that cell. The resulting distribution of vortices shows the expected axisymmetry, as well as a strong concentration of vortices in the shear layer at the boundary of the potential core. The length of each vortex is also computed in the reconstruction process, and the distribution of vortex length along the x axis is shown in FIG 14, which is constructed by partitioning vortex length into 100 values ranging from 0 to 0.04m and streamwise location into 100 values between 0 and 15D. The distribution presented in FIG 14 shows the low presence of turbulence before x=3D as well as the absence of vortices with length less than 0.006m. The density of vortices is the highest between 3D (end of potential core) and 10D. The vortex length increases as they are convected downstream.

After the vortex tracking step, time variations of geometrical properties of the vortices are computed. For example, the convection velocity of vortices is computed, as shown in the snapshot image of FIG. 15. In FIG. 15, reconstructed centerlines colored by convection velocity from 30 to 130m/s are shown. Here it can be seen that the convection velocity is almost zero in the outer layer of the jet shear layer and reaches a maximum close to the potential core boundaries. Distribution of the convection velocity along the streamwise direction is also computed. FIG. 16 shows an example graph of mean convection velocity along the x-axis. FIG. 16 shows an initial increase of the convection velocity, followed by a slow decrease moving downstream from the end of the potential core starting at ~0.3m. For convection velocity, the 99% confidence interval is relatively small compared to the mean value, about 5%. The stretching of vortices is also computed based on the length change of the vortex centerlines from frame to frame. A snapshot of the stretching of individual vortices is presented in FIG 17 (e.g., reconstructed centerlines colored by stretching from 0 to 10000%/s), and the distribution of stretching along the jet axis is presented in FIG. 18. The distribution of stretching shows a peak value of 3.5% per frame where the shear layer starts generating vortices in the outer boundary of the potential core. The stretching is then constant at about 0.7% per frame. It shows that vortices keep increasing in length as they move downstream in the jet; this is mostly due to 3 dimensional effects of the dissipation of the vortex cores.

Finally, the vortex system detection method provides information about pairs of vortices in co-rotation. At each time frame, the frequency of the sound emitted by a CRV is calculated from its rotation speed. To study the frequency-dependent CRV spatial distribution, which

corresponds to the noise source distribution, the number of CRVs whose frequency is within a pre-determined 200Hz band is calculated everywhere in the flow for frequency bands between 0 and 5kHz. This number is normalized by the unit volume of the grid cell. The obtained scalar is the noise source density. The results are presented in FIG. 19 which shows a density of noise sources for the frequency band 200-400Hz (a), 800-1000Hz(b), 2000-2200kHz (c) and 3000-3200Hz (d). The maximum density is obtained in a cell for the 800-1000Hz band range. It corresponds to the band where the maximum of far-field SPL is observed, as presented in FIG. 20 which shows simulation results for 1/3rd octave SPL at a probe located at 90° from the jet axis at x = 0.2m. The presence of vortex pairs is close to 0 for low frequencies (<200Hz) and the high frequency bands vortex pairs count is lower than in the 800-1000Hz range. Overall, the CRV noise sources are concentrated close to the potential core, where vertical eddies (thus turbulence) are generated in the shear layer.

FINSIM Application

To illustrate the capabilities of the present approach to identify flow induced noise sources, it is applied to two different cases where a difference in noise generation has been observed. The first case is the comparison of two jet nozzle designs, SMC000 (round nozzle presented in the former section) and SMC006 (chevron type nozzle), for which the geometries are shown in FIGS. 21A and 21B, respectively. The second case is the comparison of two different side-mirror designs for a fully detailed production car which are known to generate different levels of radiated acoustics.

A. Jet nozzle geometry comparison: SMC000 vs SMC006

The SMC000 simulation and analysis using FINSIM were described in section IV. The SMC006 simulation was identical except for the change of nozzle geometry. FINSIM is applied to both cases, and the resulting spatial distributions of vortices, presented in FIGS. 22A and 22B, shows interesting differences. The SMC006 vortex distribution (FIG. 22A) is more localized because the chevrons tend to collapse the potential core. In the SMC000 case (FIG. 22B), the vortices are located all along the jet, downstream and around the potential core. However in the SMC006 case, the vortices are located mainly at the end of the potential core, which extends only about half the distance in the streamwise direction compared to SMC000. The potential core is also

wider for SMC006, and vortices are distributed further in the radial direction compared to SMC000.

Further downstream, the turbulence, as indicated by the population of vortices, is rapidly dissipated for SMC006. Given the differences in vortex distribution, it can be expected that the SMC006 noise source locations are more localized, and possibly more intense at specific frequency bands.

FIG. 23 shows simulated distribution of the noise sources for the nozzle designs of FIG. 21A and 21B at different bandwidths. In FIG. 23, the distribution of noise sources (represented as before by the CRV density) is presented for SMC000 and SMC006. In order to compare the two designs, the distribution at each bandwidth is normalized by the maximum CRV density value considering both cases. These plots show that at low frequencies, the amount of CRV noise sources is larger for the SMC006 design, and localized close to the exit of the nozzle. The penetration of the nozzle chevrons in the jet triggers the turbulence, reduces the potential core length and creates the observed noise sources. Similar to the vortex distributions, the amount of CRV noise sources is relatively less for the SMC000 design and they are more evenly distributed along the plume. Up to 1200Hz, the highest noise source concentrations belong to the SMC006 design. However, at higher frequencies, the trend is reversed and the the SMC000 has the higher noise source concentrations, but they are still evenly distributed in the plume whereas the SMC006 sources are still more localized even while decreasing in number with increasing frequency. In FIG. 24 the total number of noise sources is plotted vs frequency, and this clearly shows the difference in frequency distribution of the noise sources for these two nozzle designs, with SMC006 noise sources more concentrated at low frequencies and falling off at high frequencies compared to SMC000.

For now, a comparison of the resulting radiated acoustic power is not provided because it requires computation of intensity and power of the sources. Note that so far no depiction of the strength of the vortices has been shown. Until now the computation of the centerlines was not accurate enough to obtain such quantities. New development in the centerlines algorithm and rotation detection will overcome this issue and enable the strength of the CRV sources to be factored in and the radiated acoustic power to be predicted.

B. Automotive side mirror design comparison:

The present approach is now used to compare wind noise sources for two different side mirror designs on a fully detailed, real production car. The two investigated geometries are presented in FIGS. 25A (mirror 1) and 25B (mirror 2). Previous experimental and simulation investigations concluded that mirror 1 causes higher turbulent wall pressure fluctuation levels on the side glass, but mirror 2 generates higher acoustic levels on the side glass. Evidence for this supposition comes in part from the acoustic wall pressure loads on the side glass computed using the 0k method, as seen in FIG. 26, which shows higher levels for mirror 2 at all frequencies except at 100Hz . For both mirror designs, FINSIM is applied to the PowerFLOW results and the total number of CRV noise sources over the simulation volume as a function of frequency over the simulated physical time is presented in FIG. 27. At each frequency, the number of noise sources is higher for mirror 1. Assuming that the vortex sizes and strengths, and hence the CRV strengths and resulting acoustic power per CRV, are comparable for the two cases, then the total number of noise sources will correspond well to the overall acoustic power, hence the trend predicted here by FINSIM provides the expected result that mirror 2 causes higher acoustic levels., and the results .

The distribution of noise sources is computed in the same way as for the jet example and presented in FIG. 30. In the zoomed out viewpoint, the overall noise source distribution is seen to be very similar between the two designs. At high frequency, more noise sources are present near the A-pillar in both designs, which agrees well with the known behavior of the A-pillar vortex. In the zoomed in viewpoint, the primary locations of the additional noise sources for mirror 2 are seen to be near the perimeter of the rear face of the mirror housing. In FIGS. 31 and 32, the velocity magnitude in the vicinity of the side mirrors on a horizontal plane shows a stronger recirculation downstream of mirror 2 compared to mirror 1. The area downstream the tip of mirror 2, corresponding to high velocity magnitude, extends on a larger distance compare to mirror 1. As the flow is detached earlier for mirror 1, it is consequently slower at the tip of the mirror where the recirculation happens. Since the kinetic energy is less, the resulting acoustic energy is also less as a higher kinetic energy induces stronger turbulent structures at the tip of the mirror, which are noisier. A stronger turbulent shear layer correlates with a higher density of energetic vortex pair interactions, leading to a higher density of noise producing CRV systems, and hence stronger noise generation as observed in FIG. 26 for mirror 2.

C. Additional automotive side mirror design comparison:

The following case illustrates the ability of FINSIM to pinpoint noise production discrepancies between two similar designs. The baseline mirror corresponds to a real car geometry and the Trailing Edge Extension (TEE) mirror is constructed from the baseline mirror by adding a step to the baseline (grey volume on FIG. 33B). Since the mirror geometries are very similar, the leading edge flow is expected to be unchanged by the geometry modification. Experiment shows that the levels of interior noise of the car are higher for the TEE mirror. Since the flow is unchanged on the window, the difference is due to the acoustic contribution of the flow, possibly generated in the mirror wake. Here the FINSIM analysis is performed in the wake of the mirror. A difference in the total number of CRVs is observed in FIG 34. The difference is constant over the whole range of frequency at about 25% (~2dB). FINSIM has detected a difference in the generation of the acoustics. This difference is also observed in FIG. 35 where the distribution of noise sources along x is higher at both frequency ranges for the TEE design, especially right downstream the leading edge..

In conclusion, the TEE design produces more noise due to the step added to the baseline geometry. This is illustrated in FIG. 36 as the noise source density is the highest for the TEEE design close to this additional volume. However, the noise source density levels are lower for the baseline design.

C. HVAC ducts design comparison:

The following case illustrates the application of FINSIM to a HVAC unit system in order to pinpoint the location of noise sources (aka CRVs). A real duct+vents geometry (FIG. 37) as well as a new design derived from this baseline are compared using FINSIM. The new design is obtained by modification of the ducts geometry in order to reduce fluctuations in turbulent areas. A noticeable difference in SPL levels is observed and consequently a reduced interior noise. The modifications are presented on FIGS. 38 and 39.

FINSIM successfully captures the difference in noise sources location and quantity as illustrated in FIG. 40. The total number of CRVs is different from the new design at all frequencies by a factor of 3 to 4. The new design is quieter than the baseline. In addition the

CRV density maps shown in FIG. 41 and FIG. 42 illustrate the efficiency of the geometry modification in the reduction of noise. FINSIM is pinpointing the location of the sources for the baseline, but is also able to rank them by importance for future design improvement prioritization. The area close to the vent shown in FIG. 39 c) is the area mostly responsible for the higher number of CRVs in the ducts.

By tracking the motion of vortices and co-rotating vortex pairs, the Flow-Induced Noise Source Identification Method (FINSIM) makes an explicit link between vortex dynamics and the resulting quadrupole-like noise radiation. By analyzing the temporal and spatial evolution of vortex pairs, the location, frequency, directionality and intensity of these noise sources are recovered. Simulation and analysis of the canonical 2D isolated co-rotating vortices (CRV) problem and a forced 2D shear layer flow case verify the viability of the basic concept. The noise sources are shown to be correctly located and the time evolution of their strength provides a reasonable prediction of the flow-induced noise production. The shear layer flow results also show the ability to capture the convection of the noise sources by the mean flow. Extension of the method to three dimensional flows is applied first to a turbulent jet configuration. The 3D vortex detection and tracking method is seen to enable CRV identification and to give reasonable results for the statistical distribution of vortex density and noise sources (represented for now by the CRV density). The application of FINSIM for design comparison is demonstrated for the jet with two different nozzle geometries, and for a car with two different side mirrors. In both studies, the expected overall noise source trends are correctly captured. In the side mirror comparison, FINSIM successfully provides the specific locations of the dominant aeroacoustic sources, allowing a clearer understanding for why one mirror is acoustically better than the other.

What is claimed is:

1. A method for flow-induced noise source identification, the method comprising:

simulating activity of a fluid in a volume, the activity of the fluid in the volume being simulated so as to model movement of elements within the volume;

at a first time in the fluid flow simulation, identifying a first set of vortices in a transient and turbulent flow modeled by the fluid flow;

at a second time in the fluid flow simulation that is subsequent to the first time, identifying a second set of vortices in the transient and turbulent flow;

tracking changes in the vortices by comparing the first set of discrete vortices and the second set of discrete vortices; and

identifying one or more potential sound generating vortex structures based on the tracking.

2. The method of claim 1, wherein tracking changes in the vortices comprises executing a tracking algorithm that identifies a displacement of each vortex in the first and second sets of vortices between the first time and the second time.

3. The method of claim 1, wherein identifying the first and second sets of vortices comprises identifying the first and second sets of vortices based on one or more of instantaneous pressure, vorticity, Q-criterion, and λ_2 criterion.

4. The method of claim 1, wherein identifying the one or more potential sound generating vortex structures comprises identifying co-rotating vortex pairs based on the position and displacement of vortices in the first and second sets of vortices between the first time and the second time.

5. The method of claim 4, further comprising:

for each identified co-rotating vortex pair:

determining an equivalent quadropole-like source;

determining a corresponding acoustic radiation; and

estimating the quadrupole-based far-field noise.

6. The method of claim 1, wherein identifying the one or more potential sound generating vortex structures comprises identifying vortices undergoing stretching between the first time and the second time.

7. The method of claim 1, wherein simulating activity of the fluid in the volume comprises:

performing interaction operations on the state vectors, the interaction operations modeling interactions between elements of different momentum states according to a model; and

performing first move operations of the set of state vectors to reflect movement of elements to new voxels in the volume according to the model.

8. The method of claim 1, wherein:

identifying the first set of vortices comprises identifying a first set of vortex centerlines with each centerline corresponding to an associated vortex in the first set of vortices; and

identifying the second set of vortices comprises identifying a second set of vortex centerlines with each centerline corresponding to an associated vortex in the second set of vortices.

9. The method of claim 8 wherein:

identifying the first set of vortex centerlines comprises:

identifying a plurality of self-contained isosurfaces associated with the vortices in the first set of vortices, the identified isosurfaces having λ_2 values that are less than a threshold; and

performing a triangulation calculation to determine the centerline from the self-contained isosurfaces; and

identifying the second set of vortex centerlines comprises:

identifying a plurality of self-contained isosurfaces associated with the vortices in the second set of vortices, the identified isosurfaces having λ_2 values that are less than a threshold; and

performing a triangulation calculation to determine the centerlines from the self-contained isosurfaces.

10. The method of claim 1, wherein tracking changes in the vortices comprises tracking the location and movement of the vortices.

11. The method of claim 1, further comprising predicting sound generated by the identified one or more potential sound generating vortex structures.

12. The method of claim 11, wherein predicting the sound generated by the identified one or more potential sound generating vortex structures comprises predicting the frequency, amplitude, intensity, power and location of the sound.

13. The method of claim 12, wherein predicting the sound generated by the identified one or more potential sound generating vortex structures further comprises predicting the directivity of the sound.

14. The method of claim 11, further comprising filtering the predicted sound based on frequency.

15. The method of claim 11, further comprising filtering the predicted sound based on directivity.

16. The method of claim 11, further comprising generating a density map of the predicted sound from the identified noise producing vortex structures.

17. The method of claim 11, further comprising generating a radiated acoustic power map of the predicted sound from the identified noise producing vortex structures.

18. The method of claim 1, further comprising identifying one or more regions on a surface that generate the sound generating vortex structures based at least in part on the identified one or more potential sound generating vortex structures and the simulated activity of the fluid in the volume.

19. A method for noise source identification, the method comprising:

simulating activity of a fluid in a volume to generate flow data, the activity of the fluid in the volume being simulated so as to model movement of elements within the volume;

identifying one or more potential sound generating vortex structures based on changes in vortices between a first time in the fluid flow simulation and a second time in the fluid flow simulation; and

identifying one or more regions on a surface that generate the sound generating vortex structures based at least in part on the identified one or more potential sound generating vortex structures and the generated flow data.

20. The method of claim 19, further comprising performing a geometry optimization process based on the identified one or more regions to generate a modified surface geometry.

21. The method of claim 19, wherein identifying the one or more potential sound generating vortex structures comprises:

at the first time in the fluid flow simulation, identifying a first set of vortices in a transient and turbulent flow modeled by the fluid flow;

at the second time in the fluid flow simulation that is subsequent to the first time, identifying a second set of vortices in the transient and turbulent flow;

tracking changes in the vortices by comparing the first set of discrete vortices and the second set of discrete vortices; and

identifying the one or more potential sound generating vortex structures based on the tracking.

22. The method of claim 19, wherein tracking changes in the vortices comprises executing a tracking algorithm that identifies a displacement of each vortex in the first and second sets of vortices between the first time and the second time.

23. The method of claim 19, wherein identifying the first and second sets of vortices comprises identifying the first and second sets of vortices based on one or more of instantaneous pressure, vorticity, Q-criterion, and λ_2 criterion.

24. The method of claim 19, wherein identifying the one or more potential sound generating vortex structures comprises identifying co-rotating vortex pairs based on the position and displacement of vortices in the first and second sets of vortices between the first time and the second time.

25. The method of claim 19, wherein identifying the one or more potential sound generating vortex structures comprises identifying vortices undergoing stretching between the first time and the second time.

26. The method of claim 19, further comprising predicting sound generated by the identified one or more potential sound generating vortex structures.

27. A computer system for simulating a physical process fluid flow, the system comprising:

a processor and a memory being configured to:

simulate activity of a fluid in a volume, the activity of the fluid in the volume being simulated so as to model movement of elements within the volume;

at a first time in the fluid flow simulation, identify a first set of vortices in a transient and turbulent flow modeled by the fluid flow;

at a second time in the fluid flow simulation that is subsequent to the first time, identify a second set of vortices in the transient and turbulent flow;

track changes in the vortices by comparing the first set of discrete vortices and the second set of discrete vortices; and

identify one or more potential sound generating vortex structures based on the tracking.

28. The system of claim 27, wherein:

the configurations to identify the first and second sets of vortices comprise configurations to identify the first and second sets of vortices based on one or more of instantaneous pressure, vorticity, Q-criterion, and λ_2 criterion;

the configurations to identifying the one or more potential sound generating vortex structures comprise configurations to identify one or more of co-rotating vortex pairs based on the position and displacement of vortices in the first and second sets of vortices between the first time and the second time and vortices undergoing stretching between the first time and the second time; and

the configurations to track changes in the vortices comprise configurations to execute a tracking algorithm that identifies a displacement of each vortex in the first and second sets of vortices between the first time and the second time; and

29. The system of claim 27, wherein the configurations to simulate the activity of the fluid in the volume comprise configurations to:

perform interaction operations on the state vectors, the interaction operations modeling interactions between elements of different momentum states according to a model; and

perform first move operations of the set of state vectors to reflect movement of elements to new voxels in the volume according to the model.

30. The system of claim 27, wherein:

the configurations to identify the first set of vortices comprise configurations to identify identifying a first set of vortex centerlines with each centerline corresponding to an associated vortex in the first set of vortices; and

the configurations to identify the second set of vortices comprise configurations to identify a second set of vortex centerlines with each centerline corresponding to an associated vortex in the second set of vortices.

31. The system of claim 27, wherein the processor and memory are further configured to predict sound generated by the identified one or more potential sound generating vortex structures.

32. The system of claim 27, wherein the processor and memory are further configured to identify one or more regions on a surface that generate the sound generating vortex structures based at least in part on the identified one or more potential sound generating vortex structures and the simulated activity of the fluid in the volume.

33. A computer program product tangibly embodied in a computer readable medium, the computer program product including instructions that, when executed, simulate a physical process fluid flow that includes a laminar to turbulent boundary layer transition, the computer program product configured to cause a computer to:

simulate activity of a fluid in a volume, the activity of the fluid in the volume being simulated so as to model movement of elements within the volume;

at a first time in the fluid flow simulation, identify a first set of vortices in a transient and turbulent flow modeled by the fluid flow;

at a second time in the fluid flow simulation that is subsequent to the first time, identify a second set of vortices in the transient and turbulent flow;

track changes in the vortices by comparing the first set of discrete vortices and the second set of discrete vortices; and

identify one or more potential sound generating vortex structures based on the tracking.

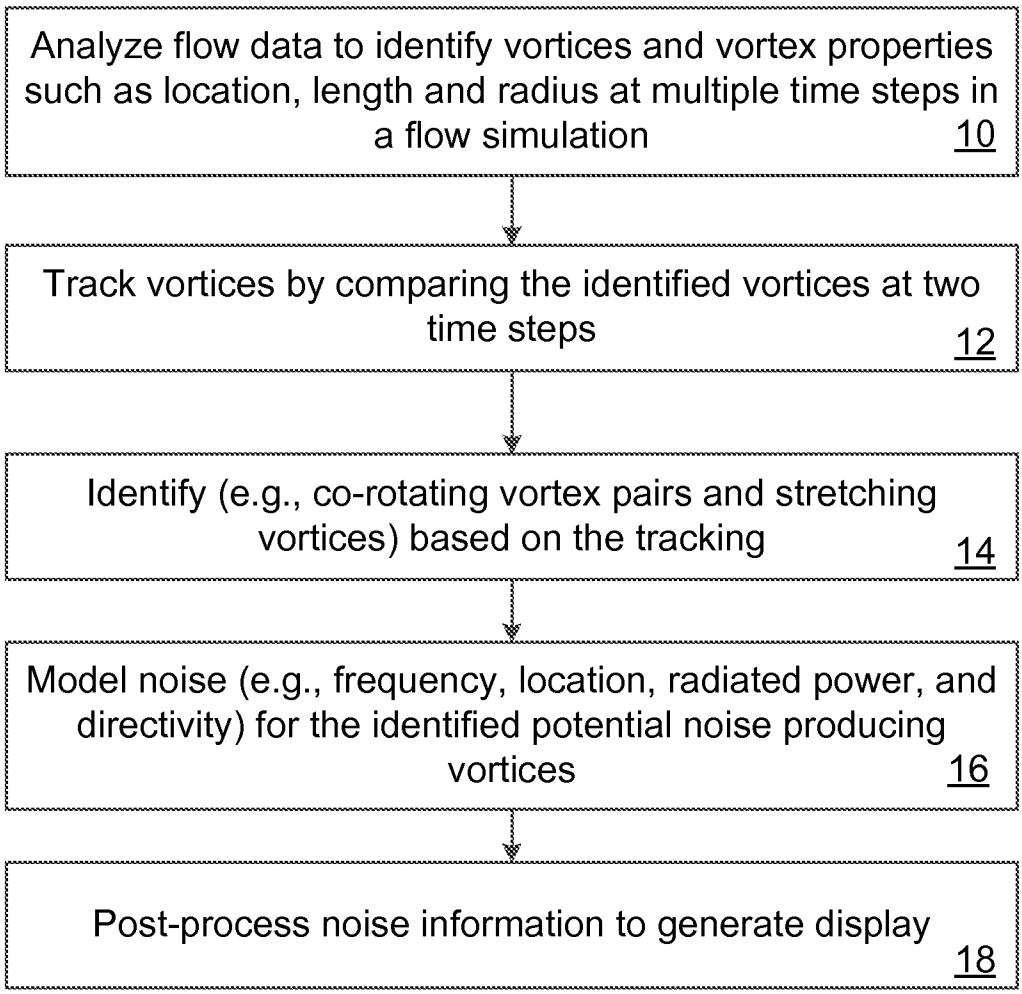
Analyze flow data to identify vortices and vortex properties such as location, length and radius at multiple time steps in a flow simulation 10
Track vortices by comparing the identified vortices at two time steps 12
Identify (e.g., co-rotating vortex pairs and stretching vortices) based on the tracking 14
Model noise (e.g., frequency, location, radiated power, and directivity) for the identified potential noise producing vortices 16
Post-process noise information to generate display 18

FIG. 1A

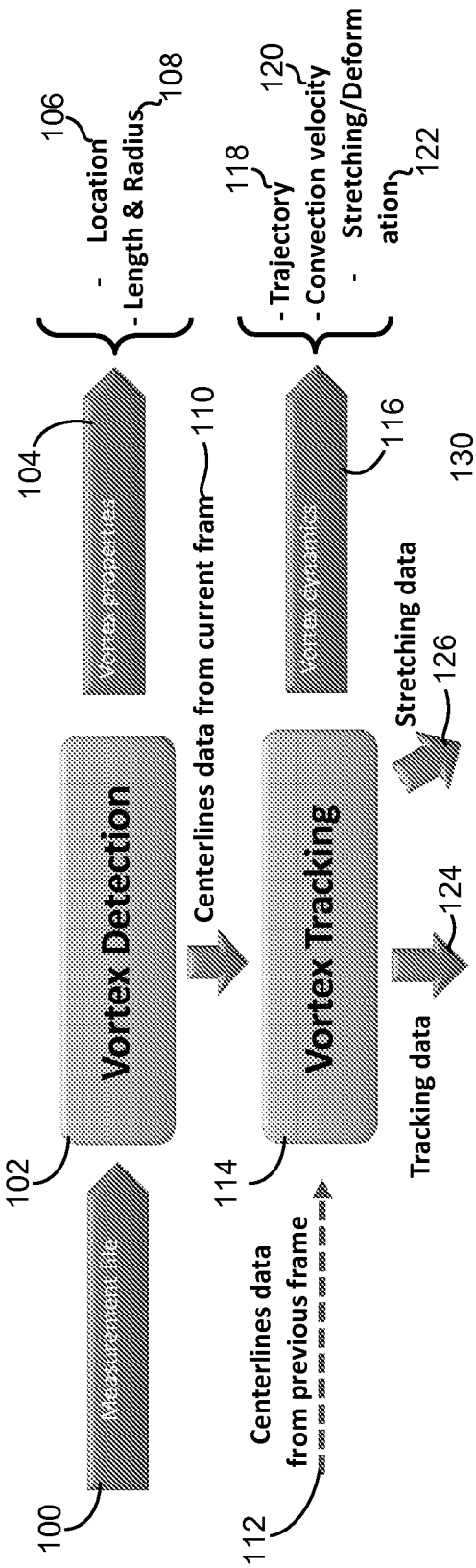
Vortex Detection
Vortex Tracking
Rotation Noise
Stretching Noise
Vortex characteristics
Centerlines data from current frame
Centerlines data from previous frame
Tracking data
Stretching data
- Location
- Length & Radius
- Trajectory
- Convection velocity
- Stretching/Deformation
134- Frequency
136- Location
138- Directivity
140- Radiated power
100
102
104
106
108
110
112
114
116
118
120
122
124
126
128
130
132

FIG. 1B

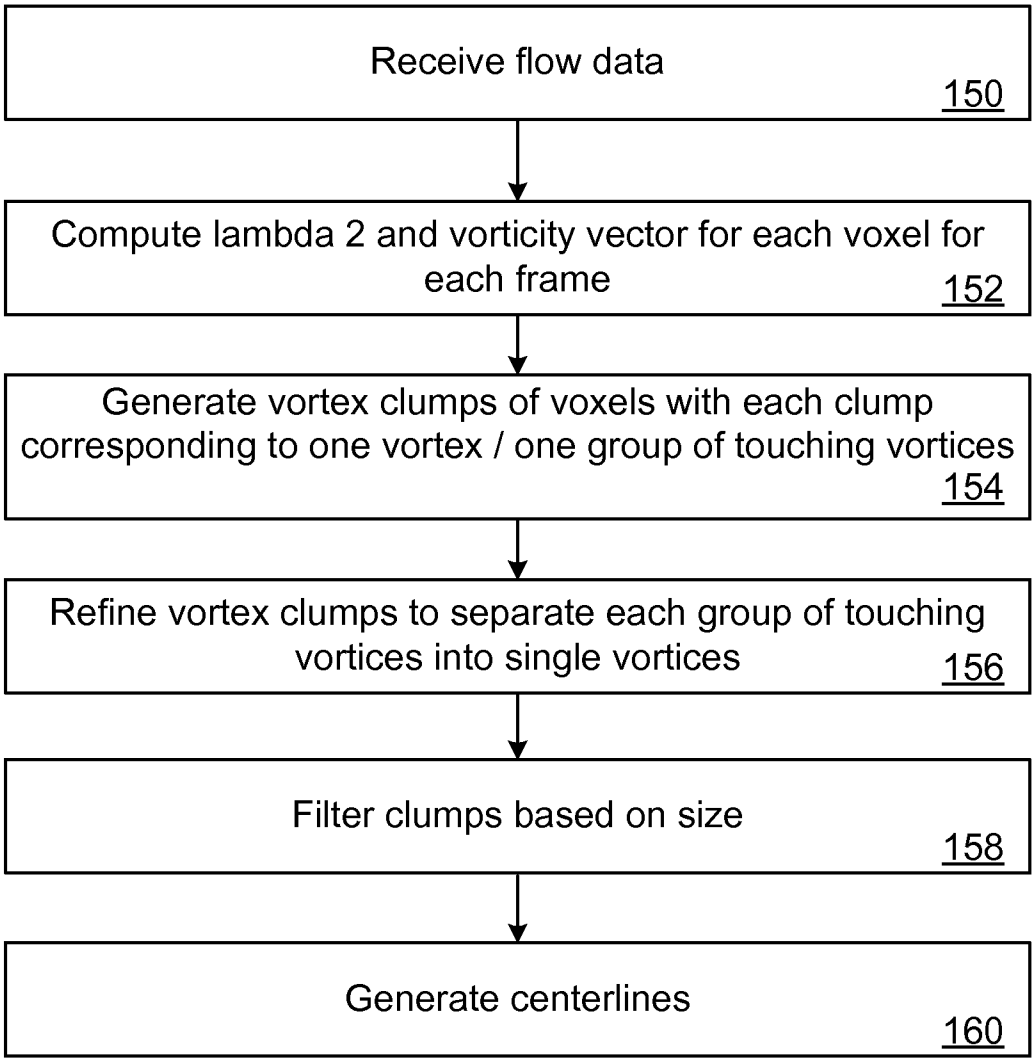
Receive flow data
150
Compute lambda 2 and vorticity vector for each voxel for each frame
152
Generate vortex clumps of voxels with each clump corresponding to one vortex / one group of touching vortices
154
Refine vortex clumps to separate each group of touching vortices into single vortices
156
Filter clumps based on size
158
Generate centerlines
160

FIG. 1C

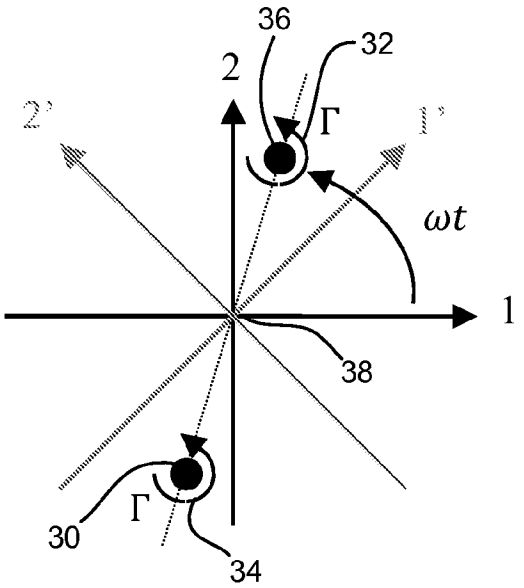

FIG. 2A

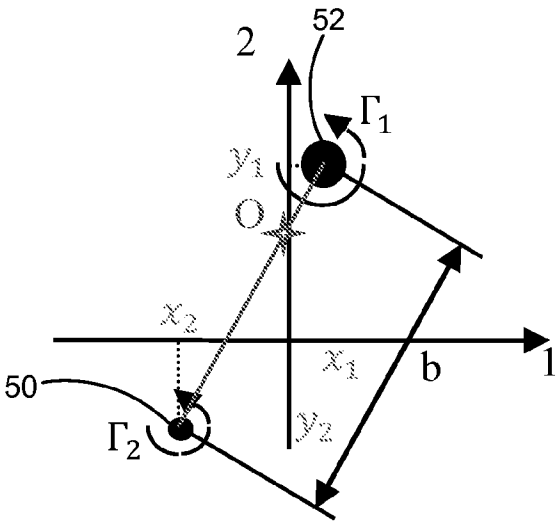

FIG. 2B

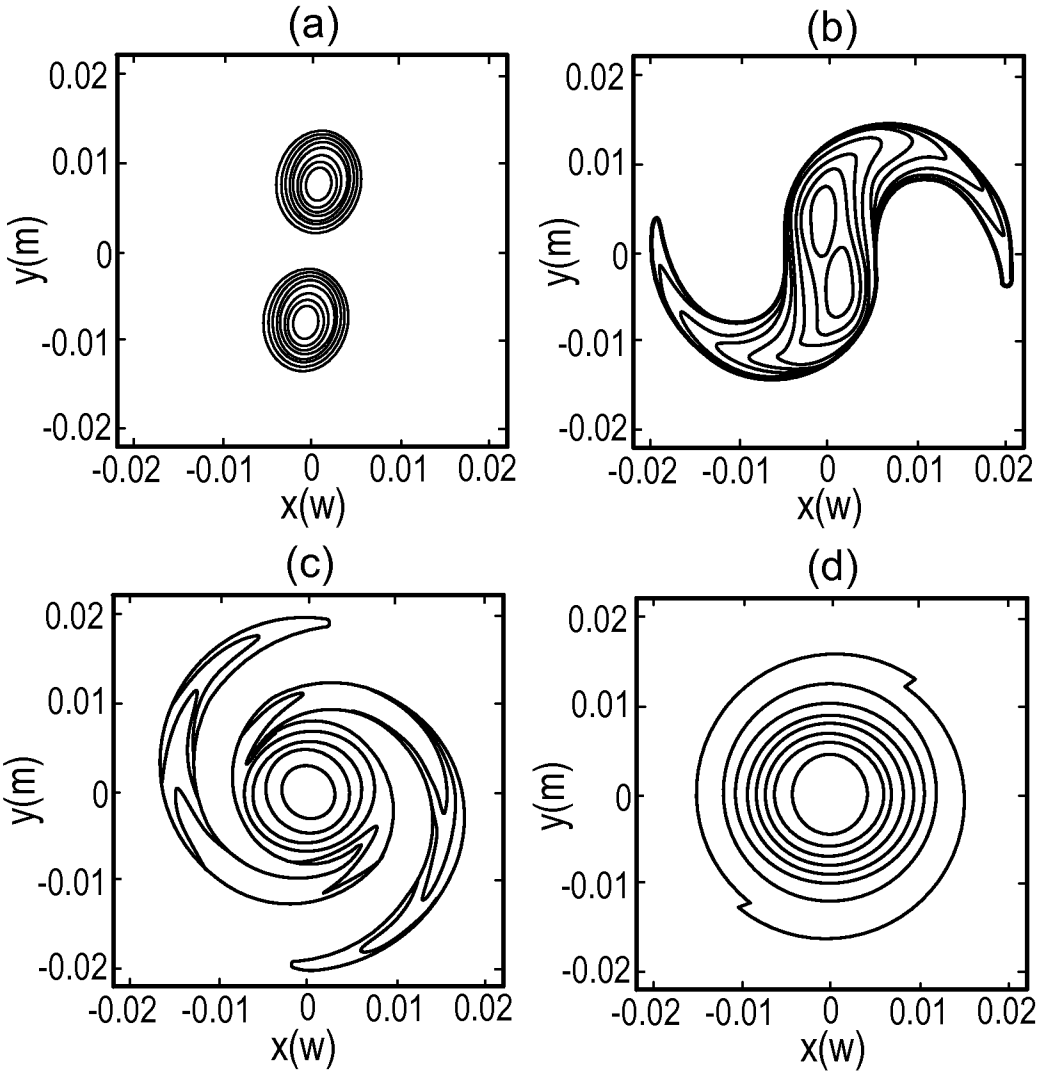
(a)
(b)
(c)
(d)
0.02
0.01
0
-0.01
-0.02
y(m)
-0.02 -0.01 0 0.01 0.02
x(w)

FIG. 3

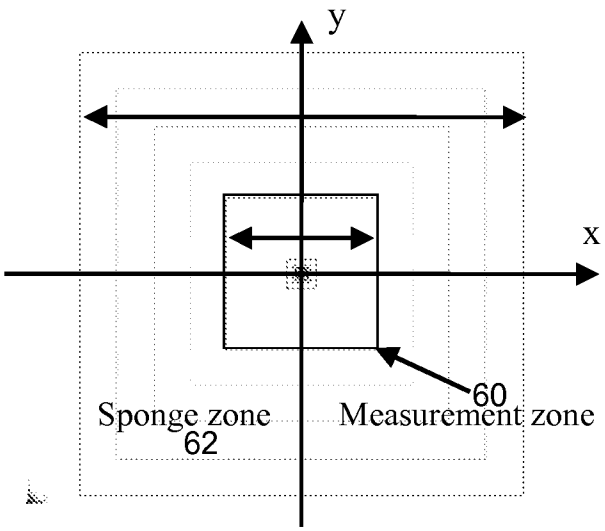
y
x
60
Sponge zone
62
Measurement zone

FIG. 4

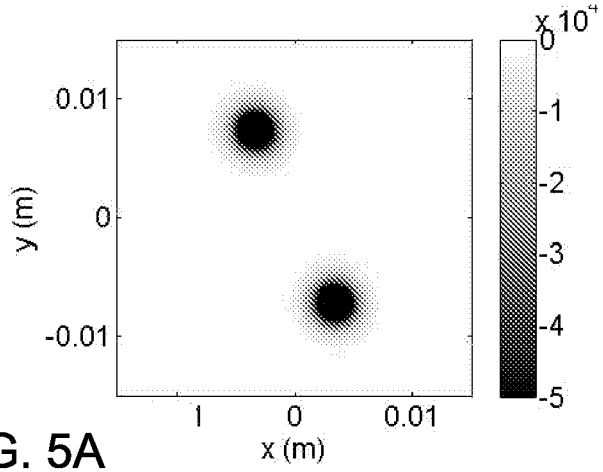

FIG. 5A

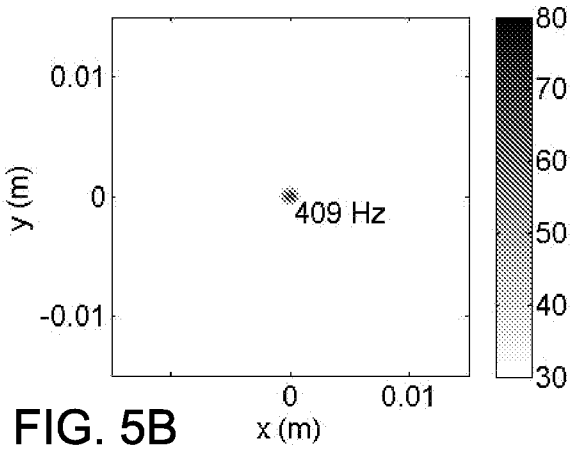

FIG. 5B

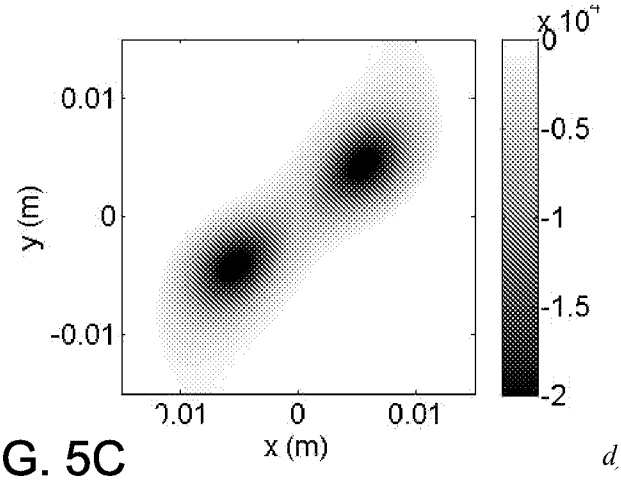

FIG. 5C

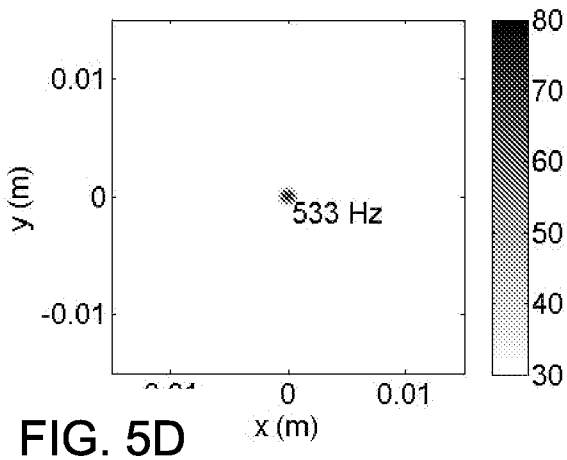

FIG. 5D

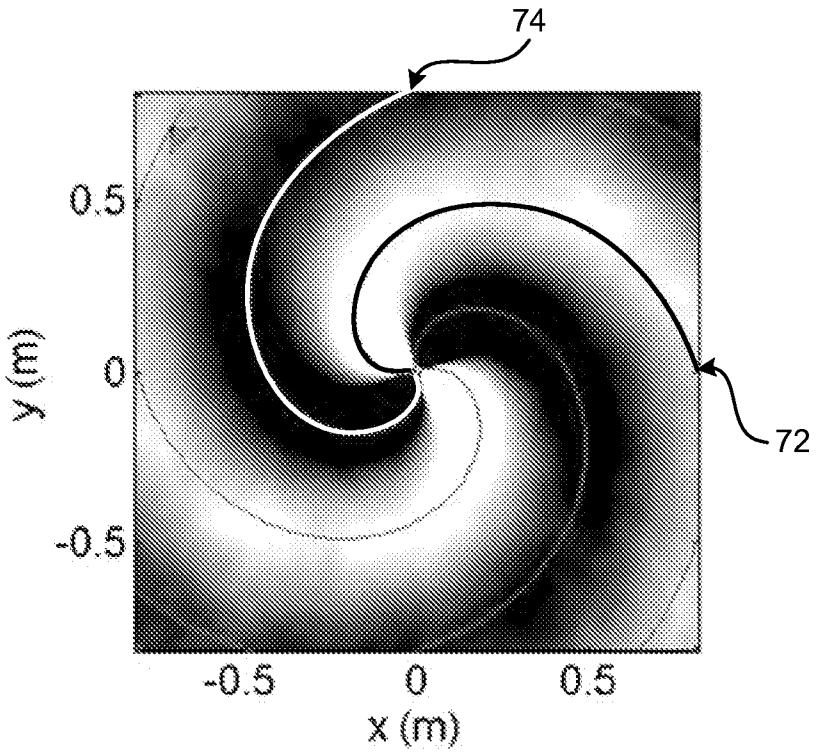

FIG. 6

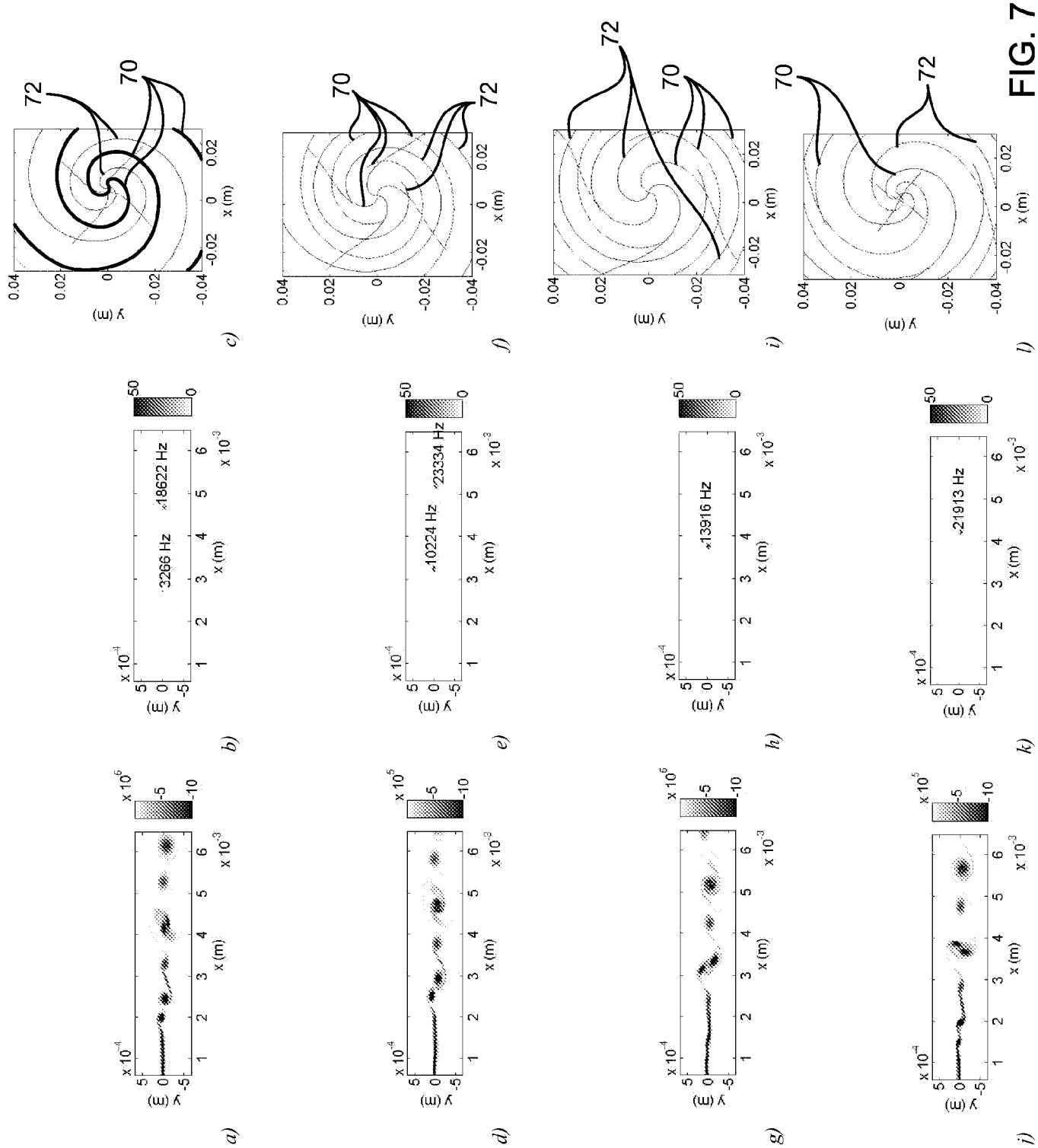
a)
b)
3266 Hz
18622 Hz
c)
72
70
d)
e)
10224 Hz
23334 Hz
f)
g)
13916 Hz
h)
i)
j)
21913 Hz
k)
l)
x (m)
y (m)

FIG. 7

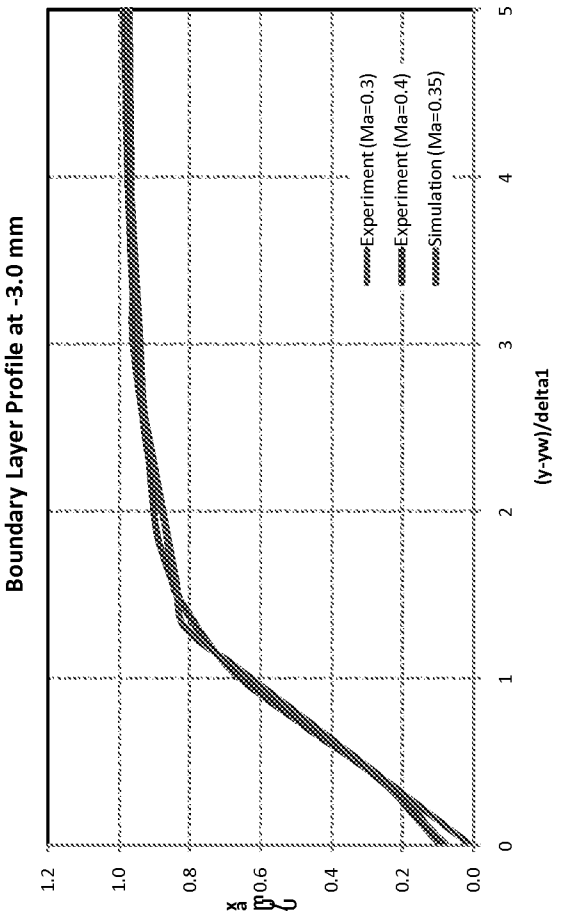
Boundary Layer Profile at -3.0 mm
Experiment (Ma=0.3)
Experiment (Ma=0.4)
Simulation (Ma=0.35)
u/U
(y-yw)/delta1
0.0
0.2
0.4
0.6
0.8
1.0
1.2
0
1
2
3
4
5

FIG. 8B

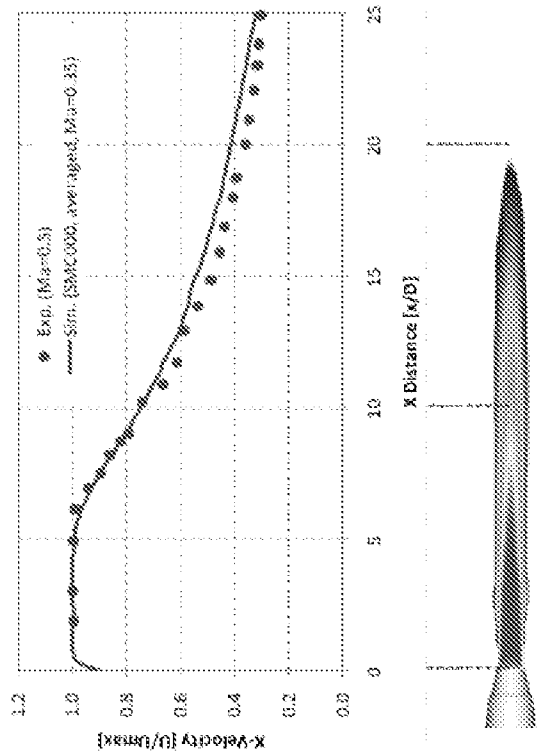
Exp. (Ma=0.3)
Sim. (SMC000, averaged, Ma=0.35)
X-Velocity [U/Umax]
X Distance [x/D]
0.0
0.2
0.4
0.6
0.8
1.0
1.2
0
5
10
15
20
25

FIG. 8A

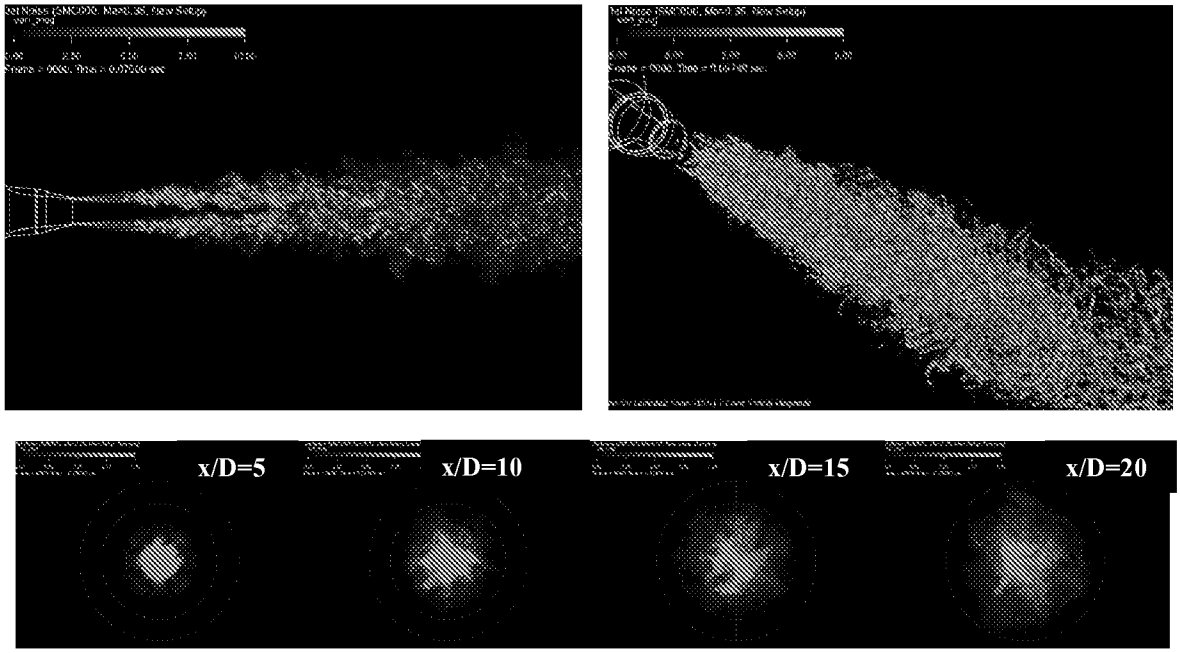

FIG. 9

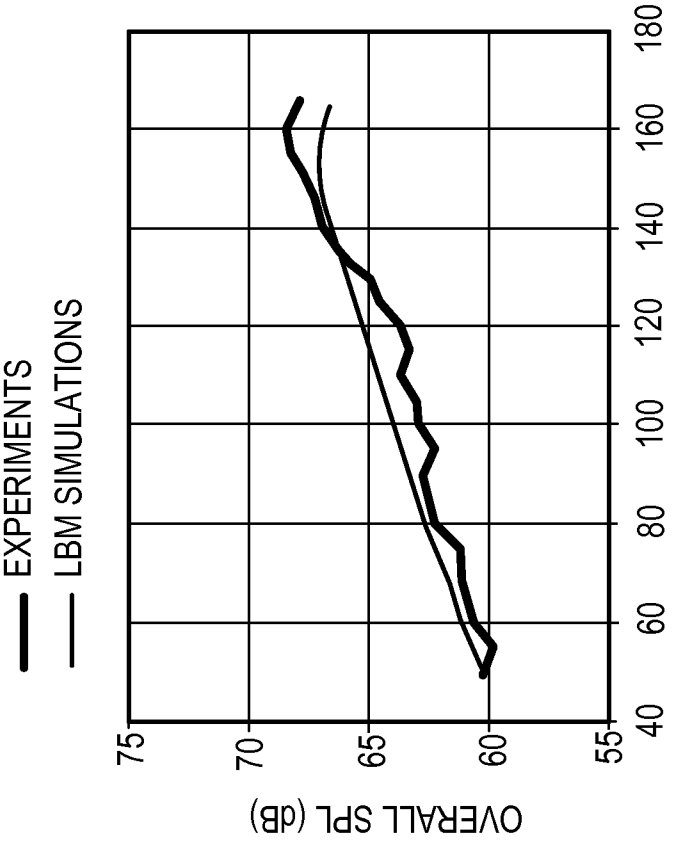

FIG. 10B

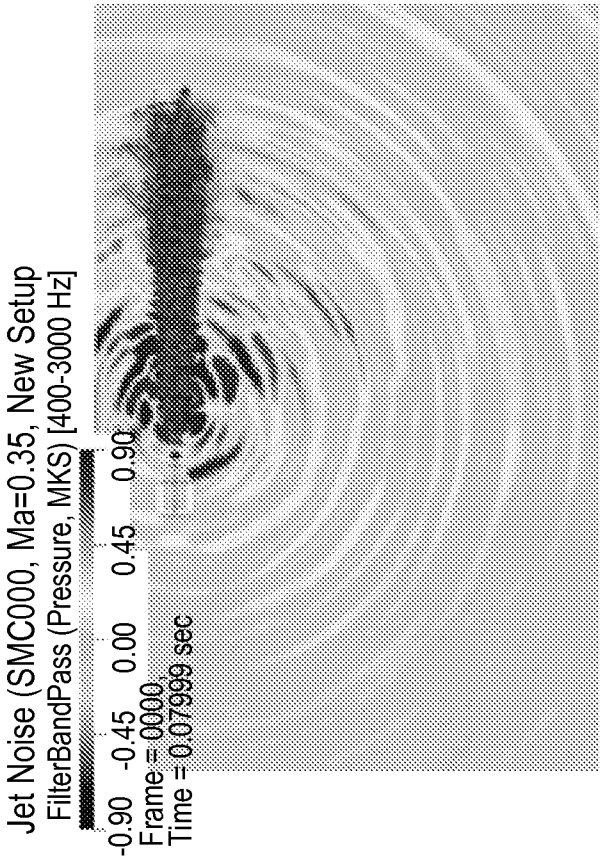

FIG. 10A

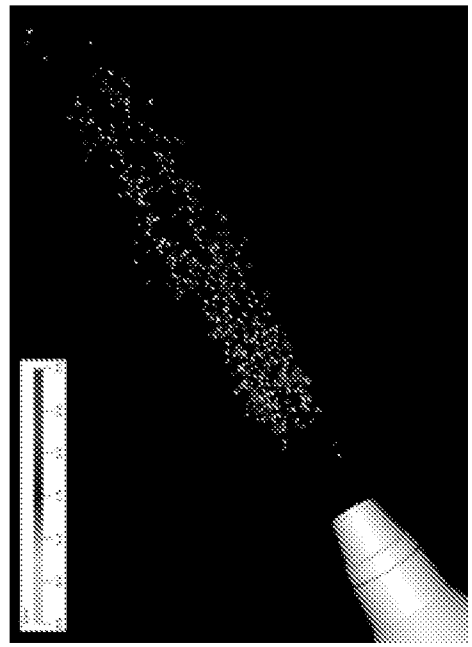

FIG. 12

FIG. 11

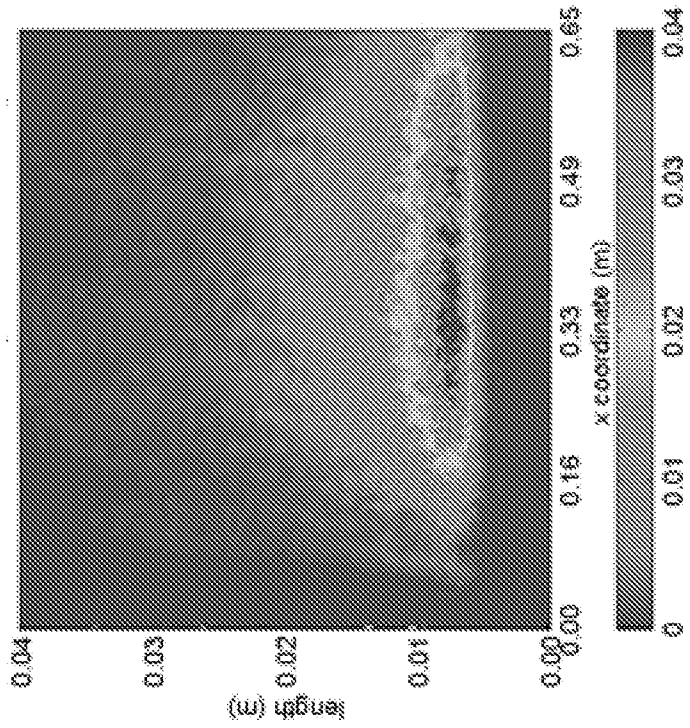

FIG. 14

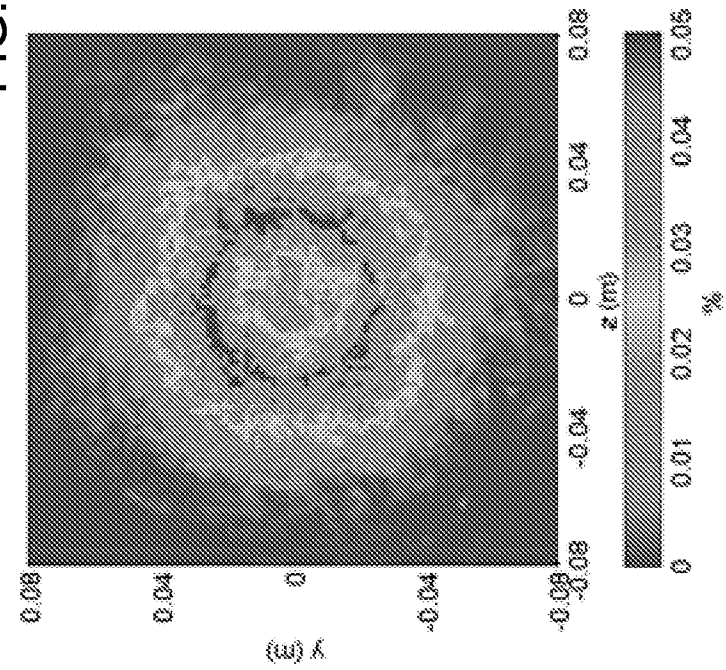

FIG. 13

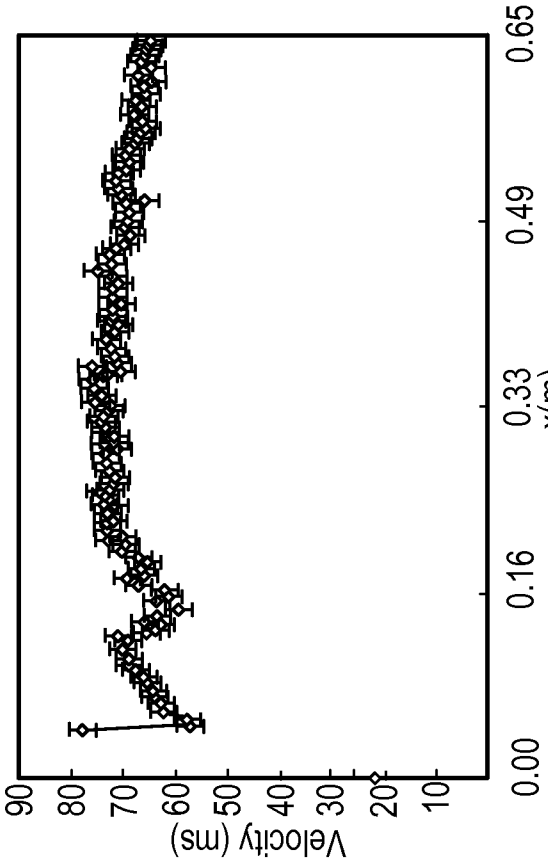

FIG. 16

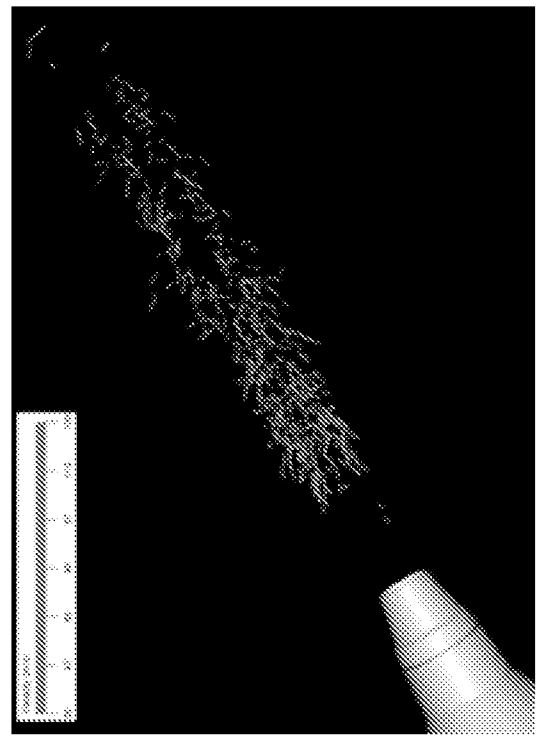

FIG. 15

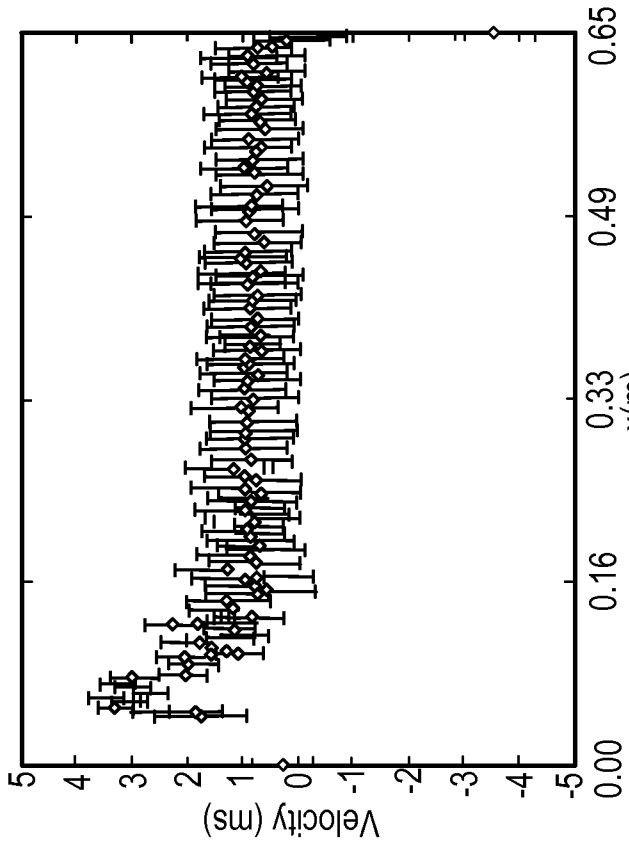

FIG. 18

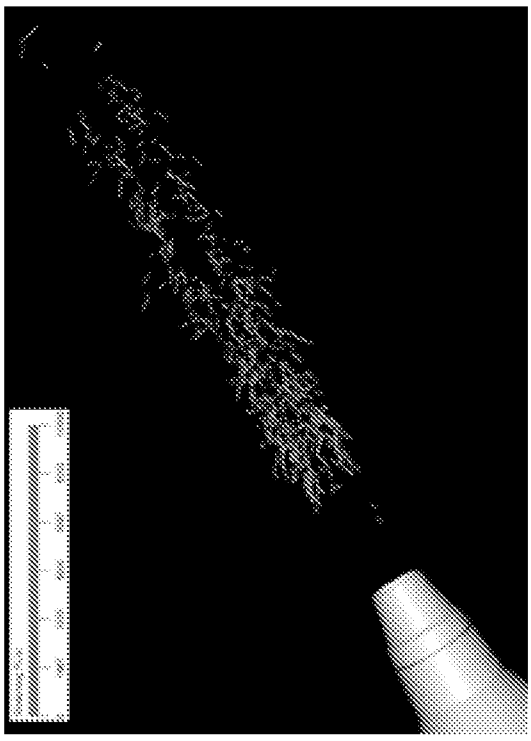

FIG. 17

FIG. 19A

FIG. 19B

FIG. 19C

FIG. 19D

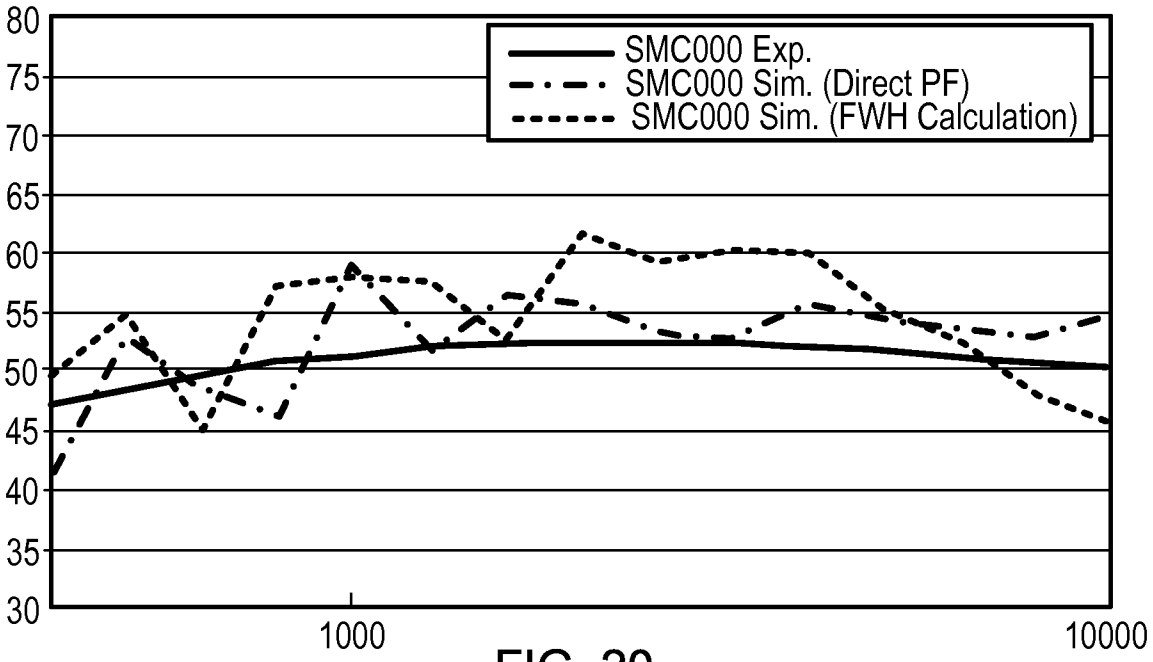

FIG. 20

FIG. 21A

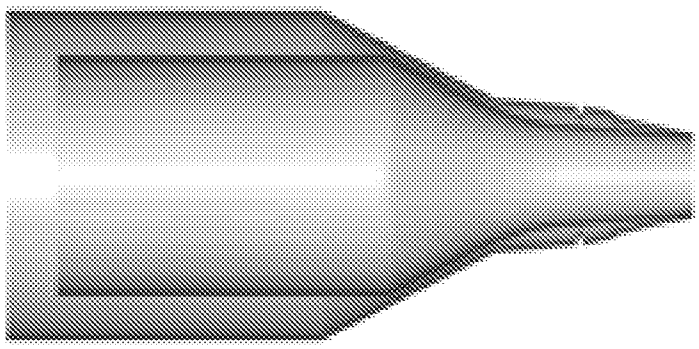

FIG. 21B

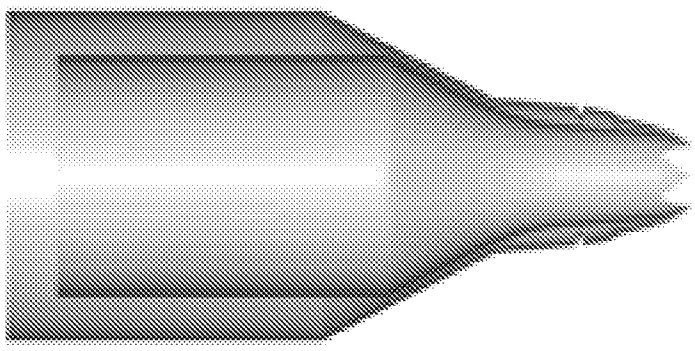

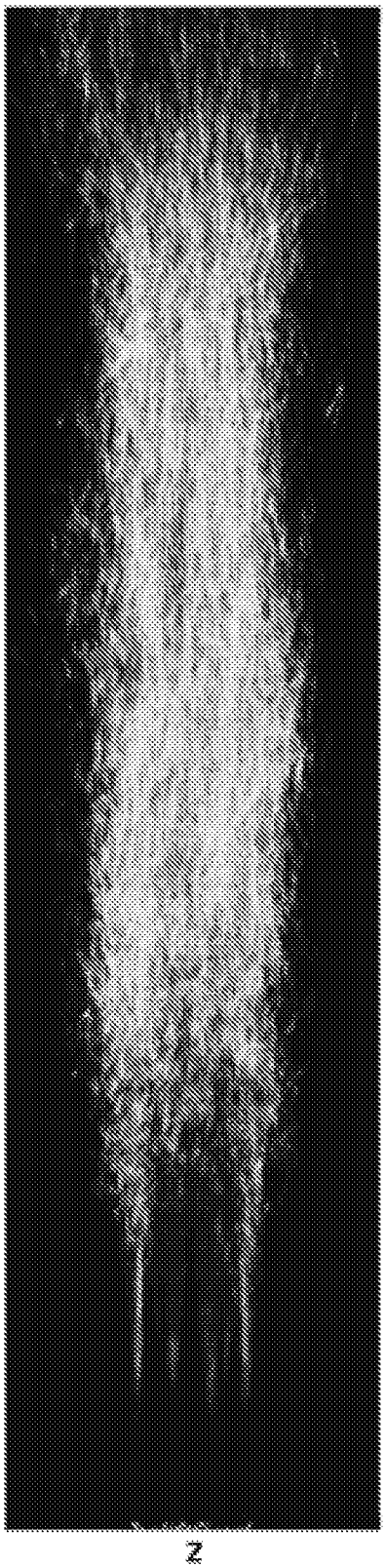

FIG. 22A

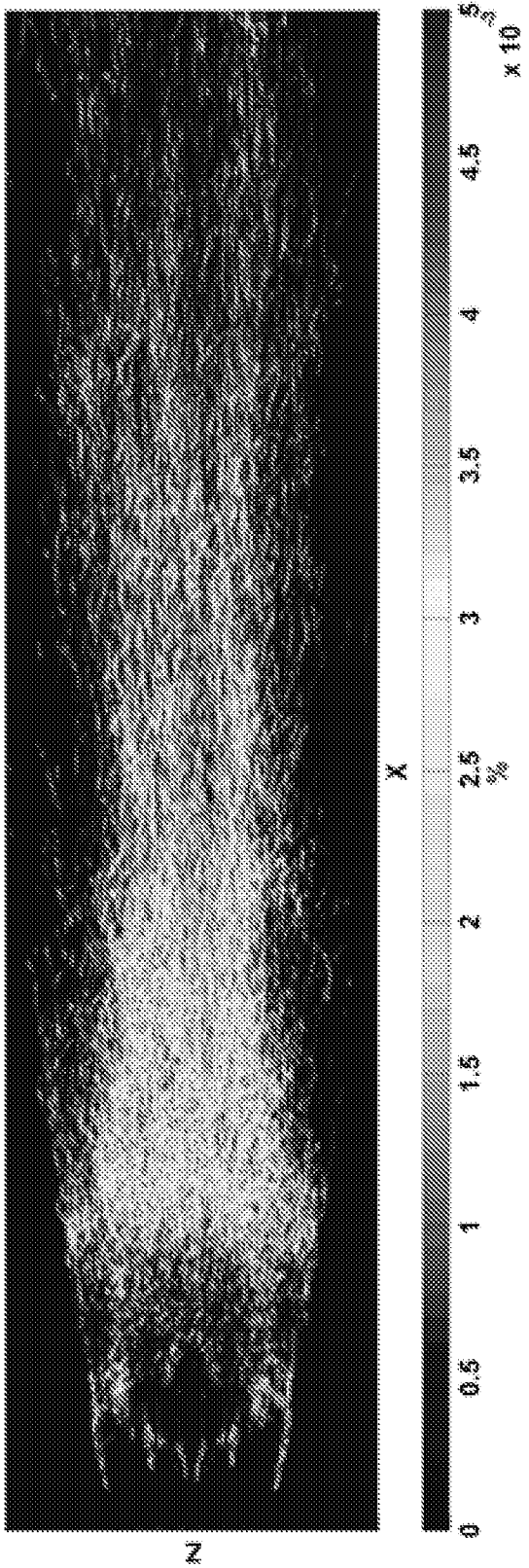

FIG. 22B

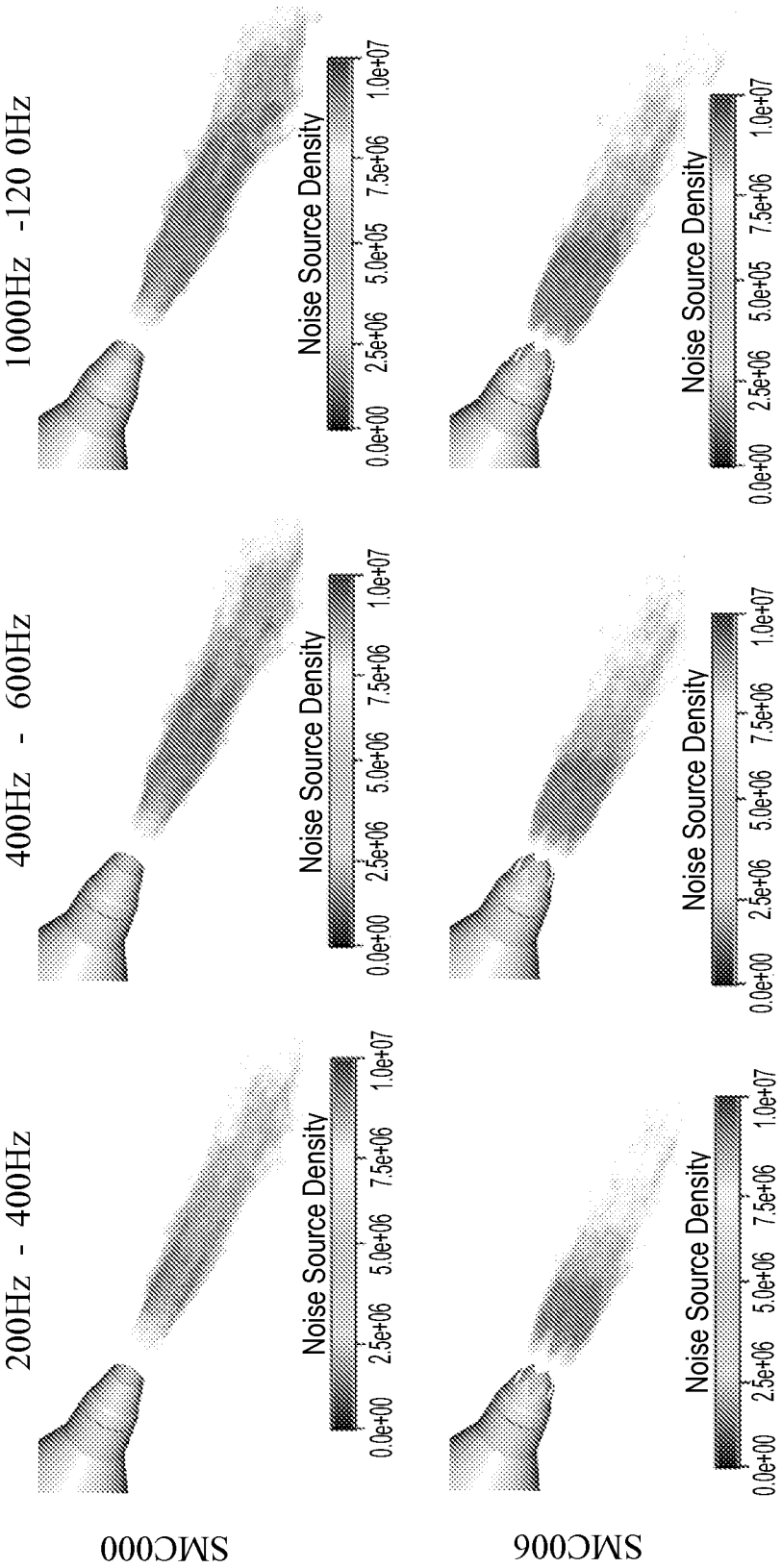
200Hz - 400Hz
400Hz - 600Hz
1000Hz -120 0Hz
SMC000
SMC006
Noise Source Density
0.0e+00
2.5e+06
5.0e+06
7.5e+06
1.0e+07
Noise Source Density
0.0e+00
2.5e+06
5.0e+05
7.5e+06
1.0e+07

FIG. 23

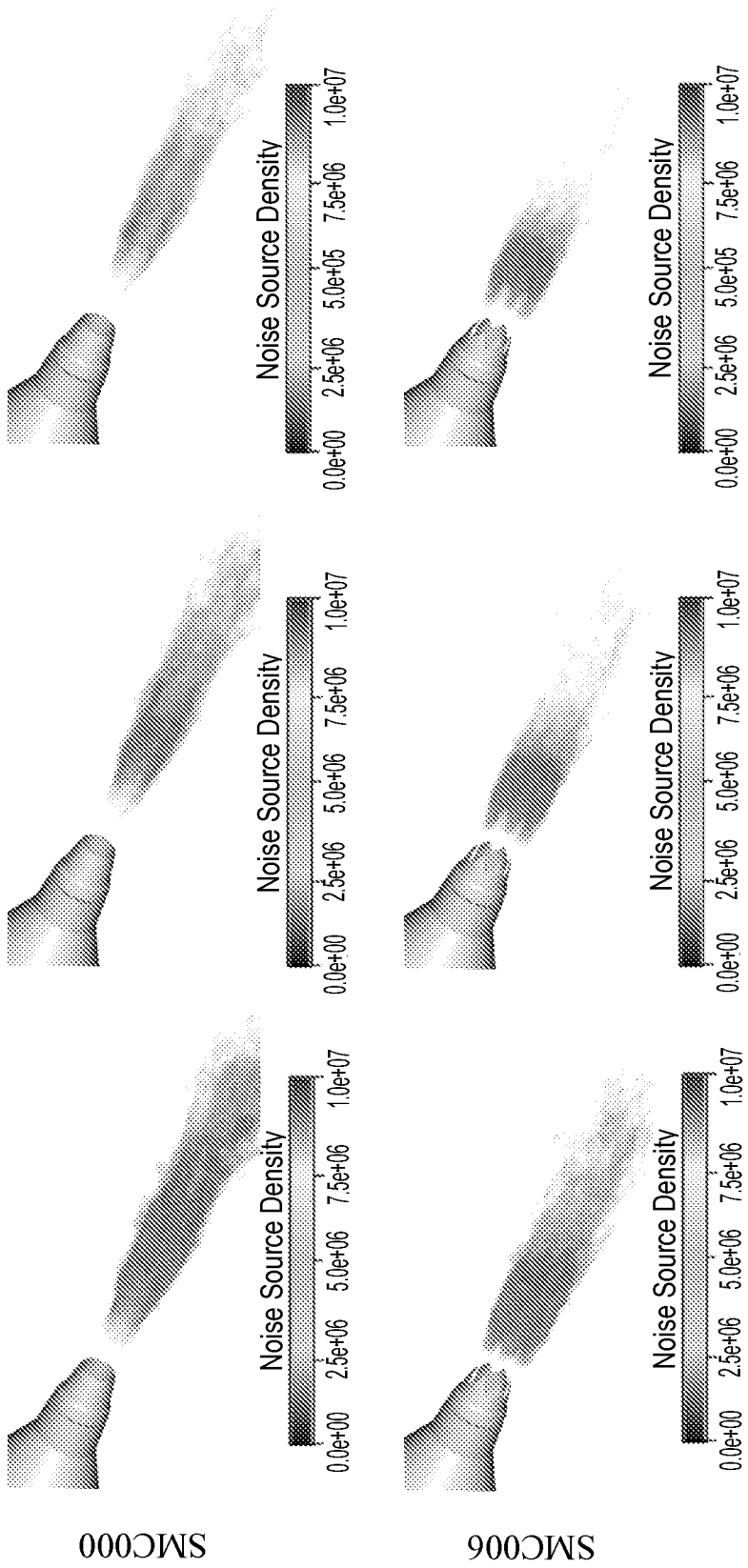
1400Hz-1600Hz
3000Hz-3200Hz
4000Hz-4200Hz
SMC000
SMC006
Noise Source Density
0.0e+00
2.5e+06
5.0e+06
7.5e+06
1.0e+07
Noise Source Density
0.0e+00
2.5e+06
5.0e+05
7.5e+06
1.0e+07

FIG. 23 (CONT)

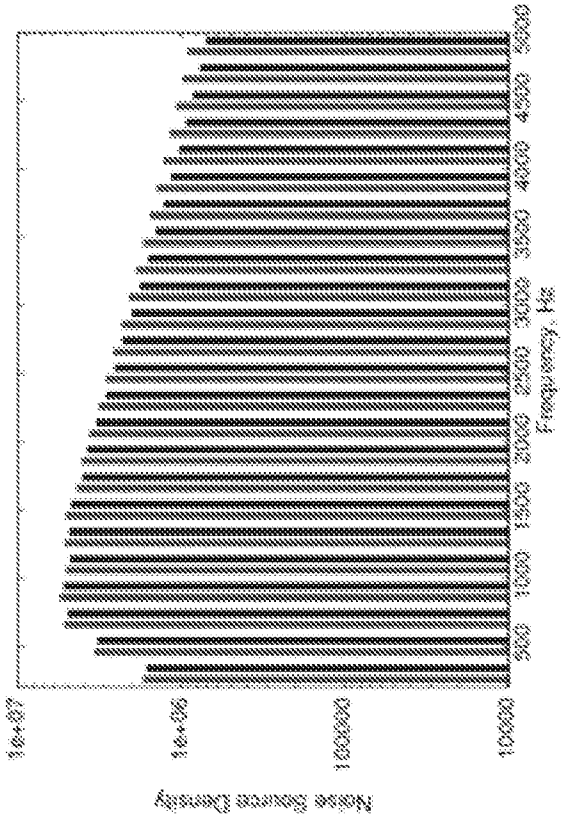

FIG. 24

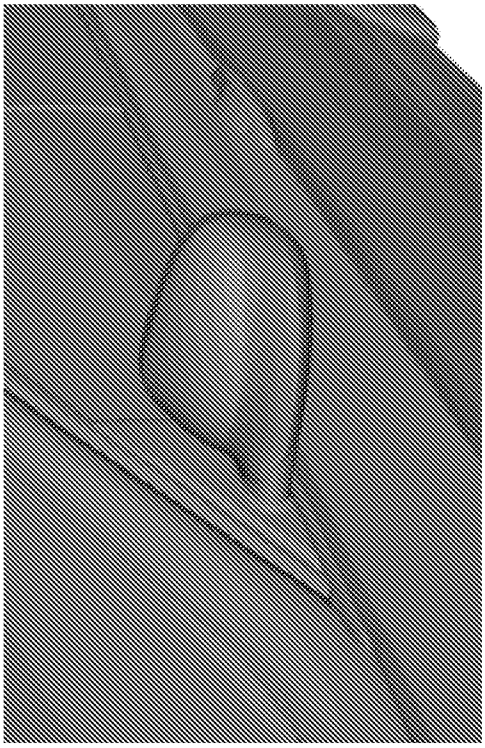

FIG. 25B

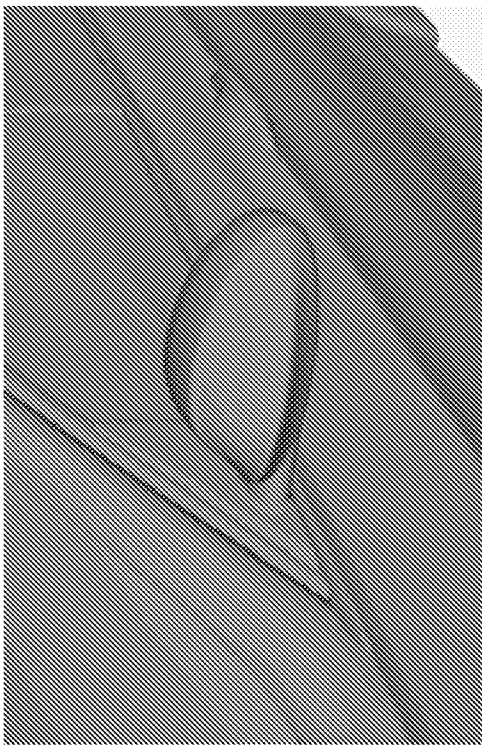

FIG. 25A

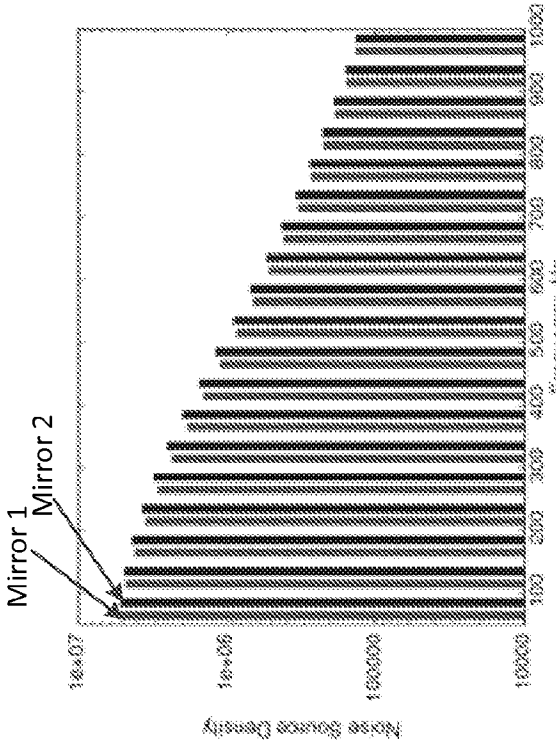

FIG. 27

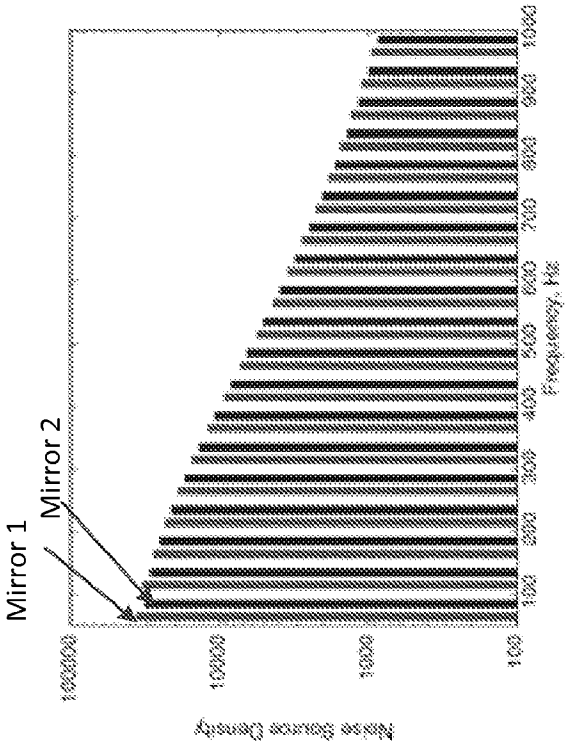

FIG. 29

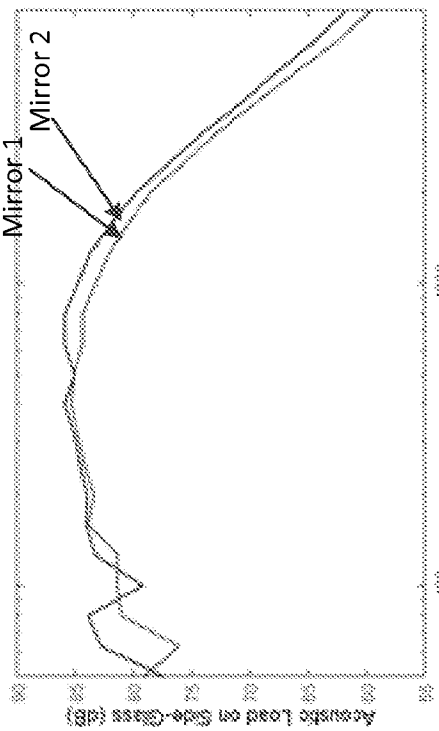

FIG. 26

FIG. 28

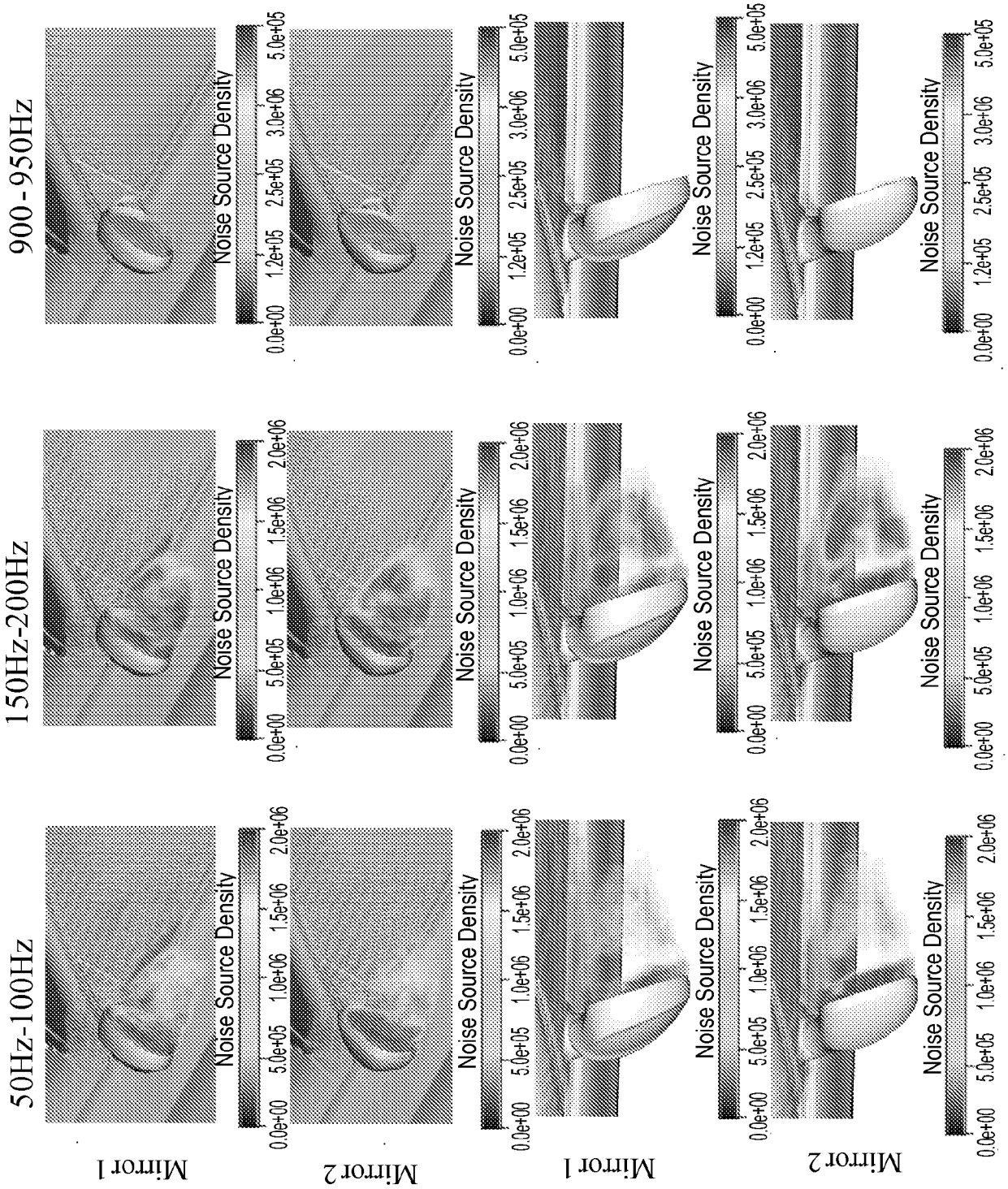
50Hz-100Hz
150Hz-200Hz
900-950Hz
Mirror 1
Mirror 2
Noise Source Density
0.0e+00
5.0e+05
1.0e+06
1.5e+06
2.0e+06
2.5e+05
3.0e+06
5.0e+05
1.2e+05

FIG. 30

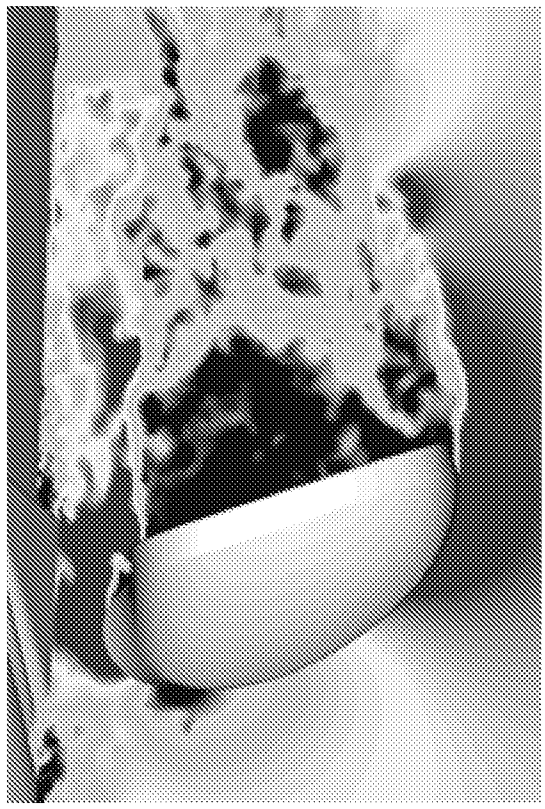

FIG. 32

FIG. 31

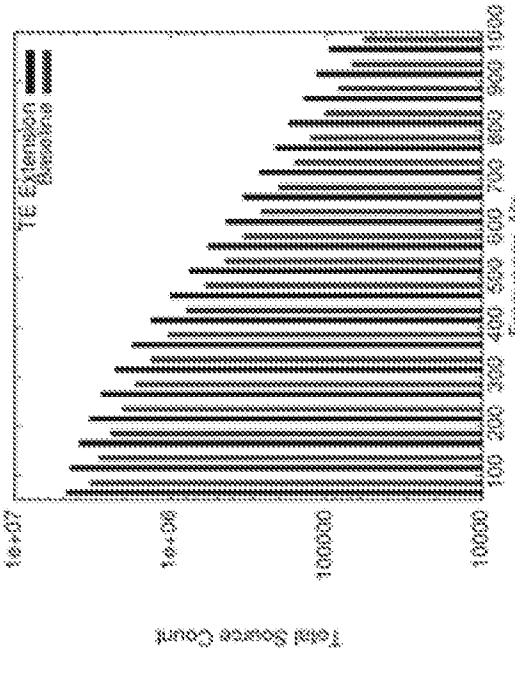

FIG. 34

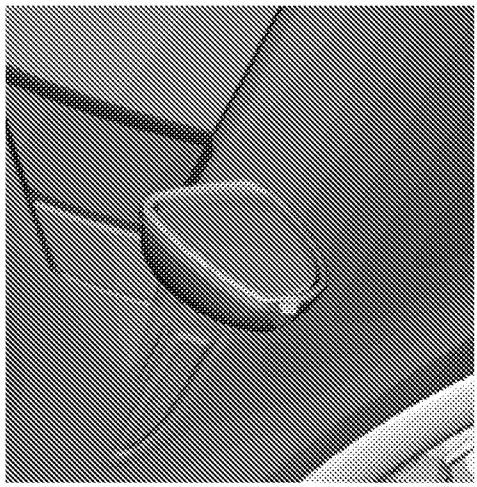

FIG. 33B

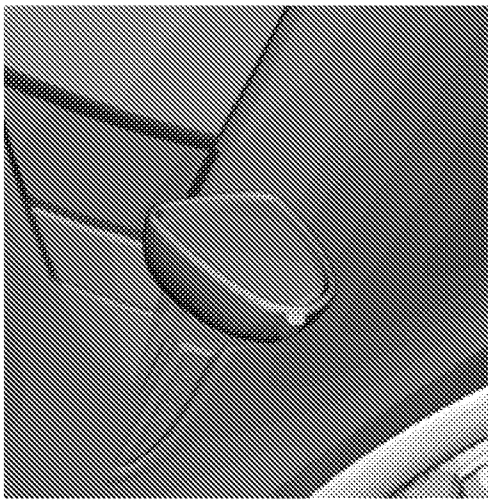

FIG. 33A

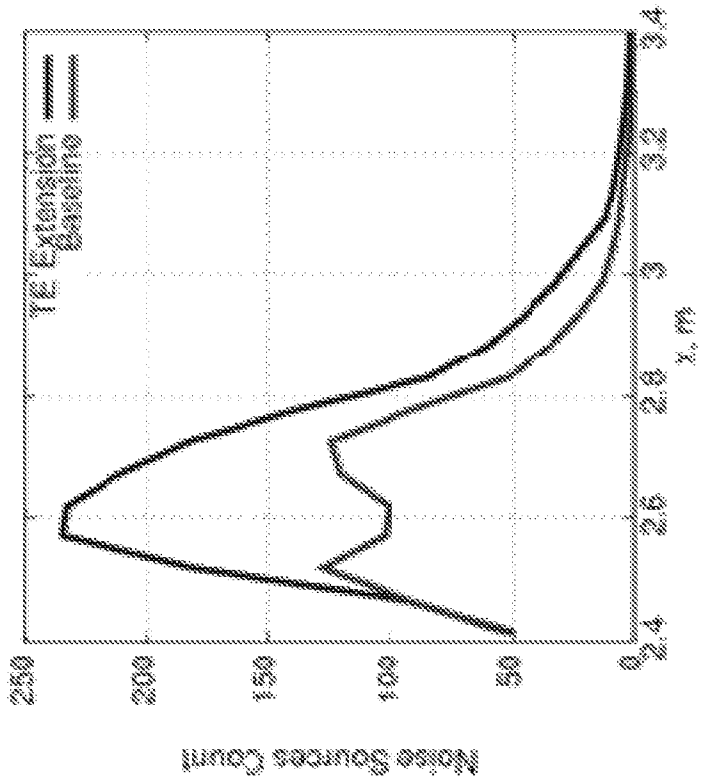

FIG. 35B

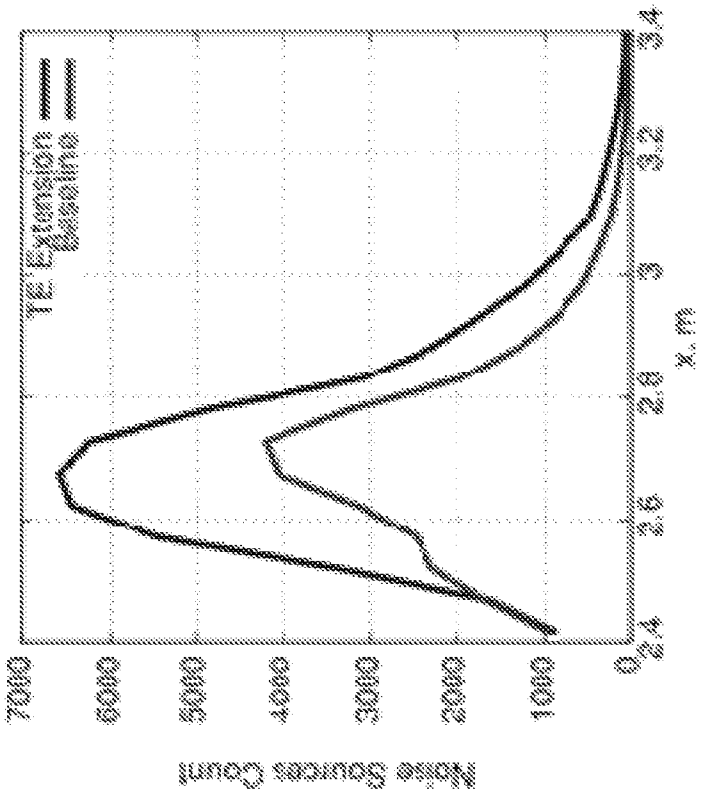

FIG. 35A

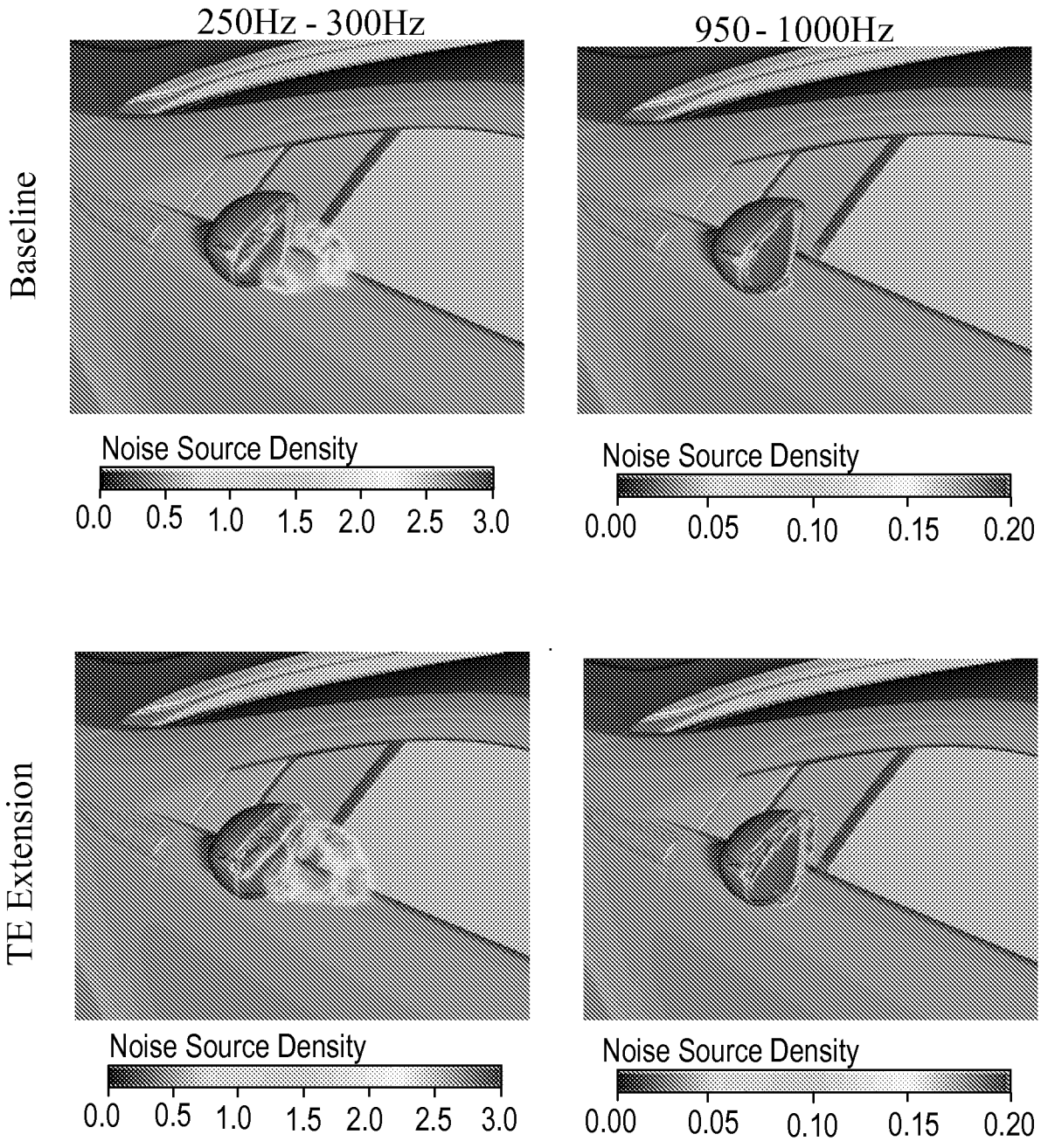
250Hz - 300Hz
950 - 1000Hz
Baseline
Noise Source Density
0.0 0.5 1.0 1.5 2.0 2.5 3.0
Noise Source Density
0.00 0.05 0.10 0.15 0.20
TE Extension
Noise Source Density
0.0 0.5 1.0 1.5 2.0 2.5 3.0
Noise Source Density
0.00 0.05 0.10 0.15 0.20

FIG. 36

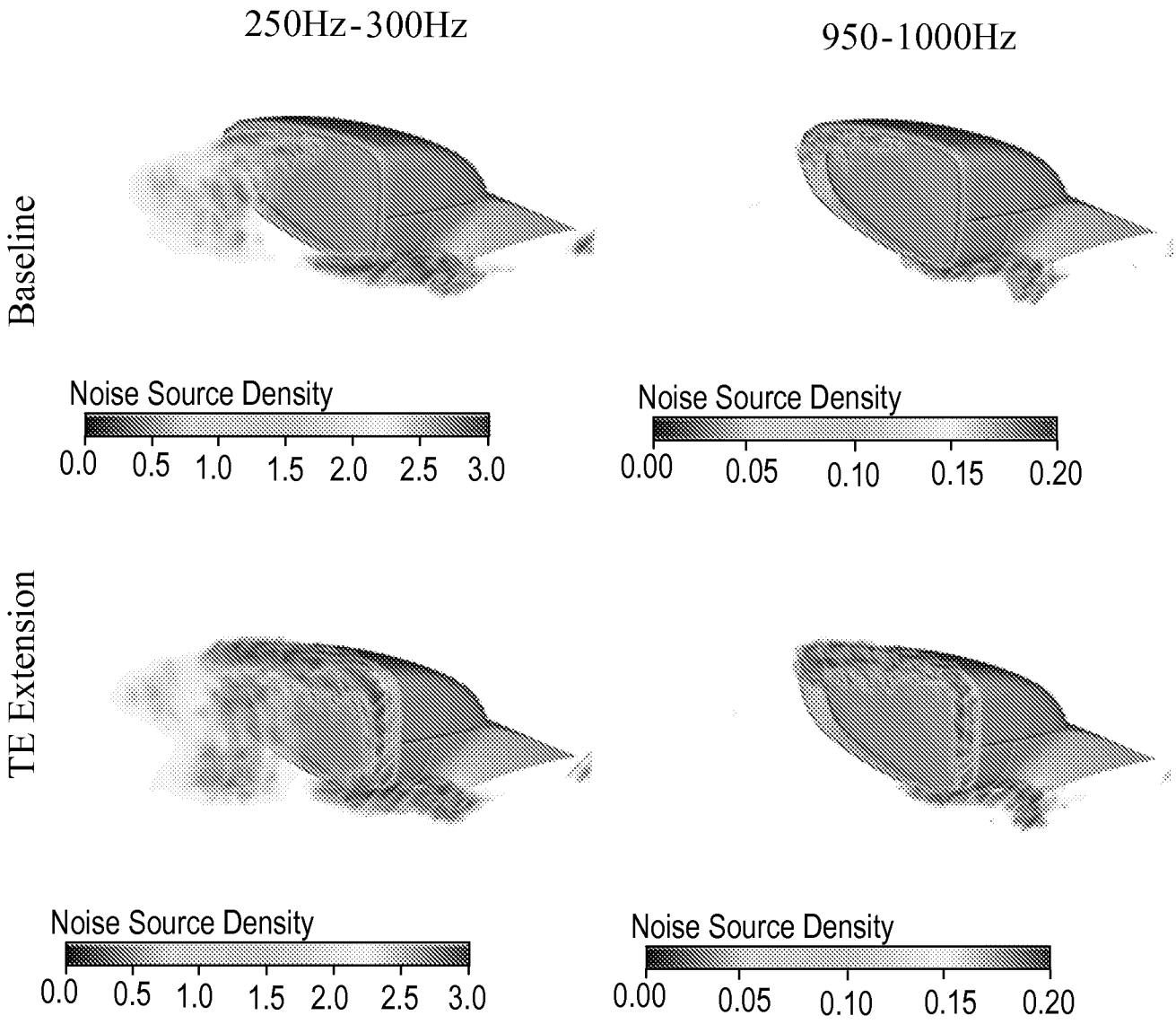
250Hz-300Hz
950-1000Hz
Baseline
Noise Source Density
0.0 0.5 1.0 1.5 2.0 2.5 3.0
Noise Source Density
0.00 0.05 0.10 0.15 0.20
TE Extension
Noise Source Density
0.0 0.5 1.0 1.5 2.0 2.5 3.0
Noise Source Density
0.00 0.05 0.10 0.15 0.20

FIG. 36 (CONT)

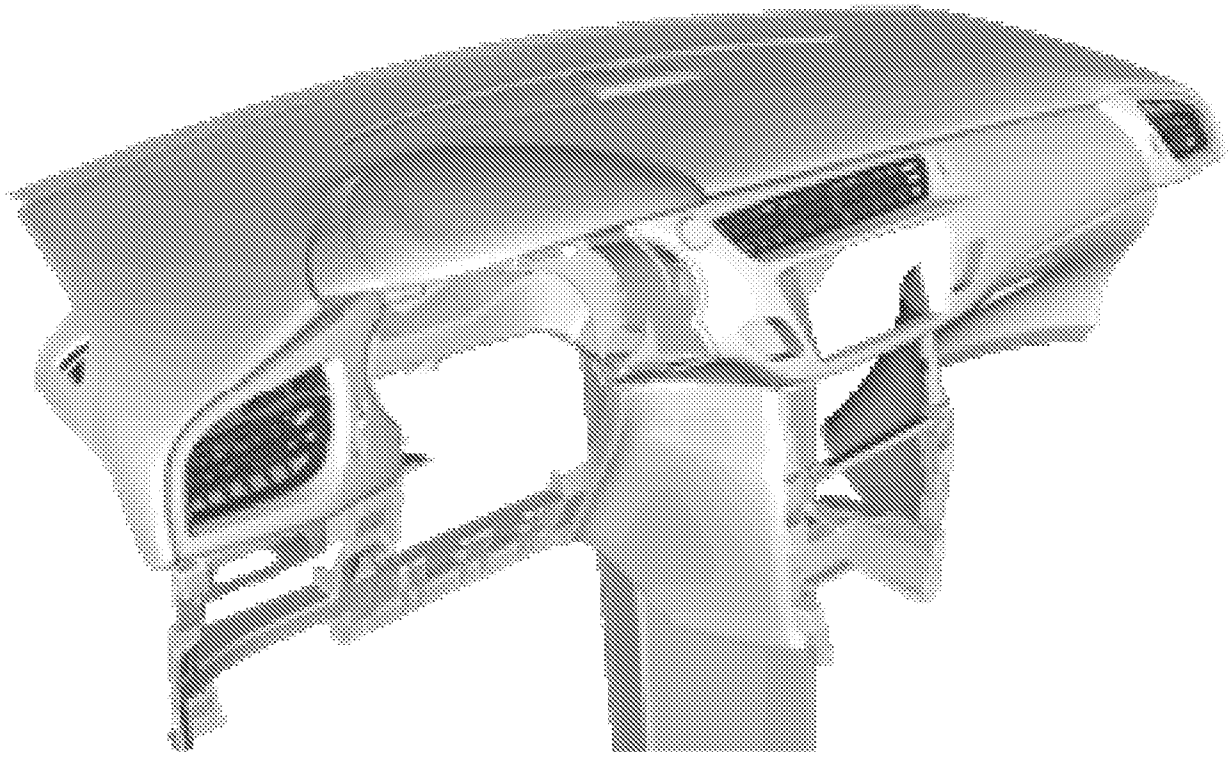

FIG. 37A

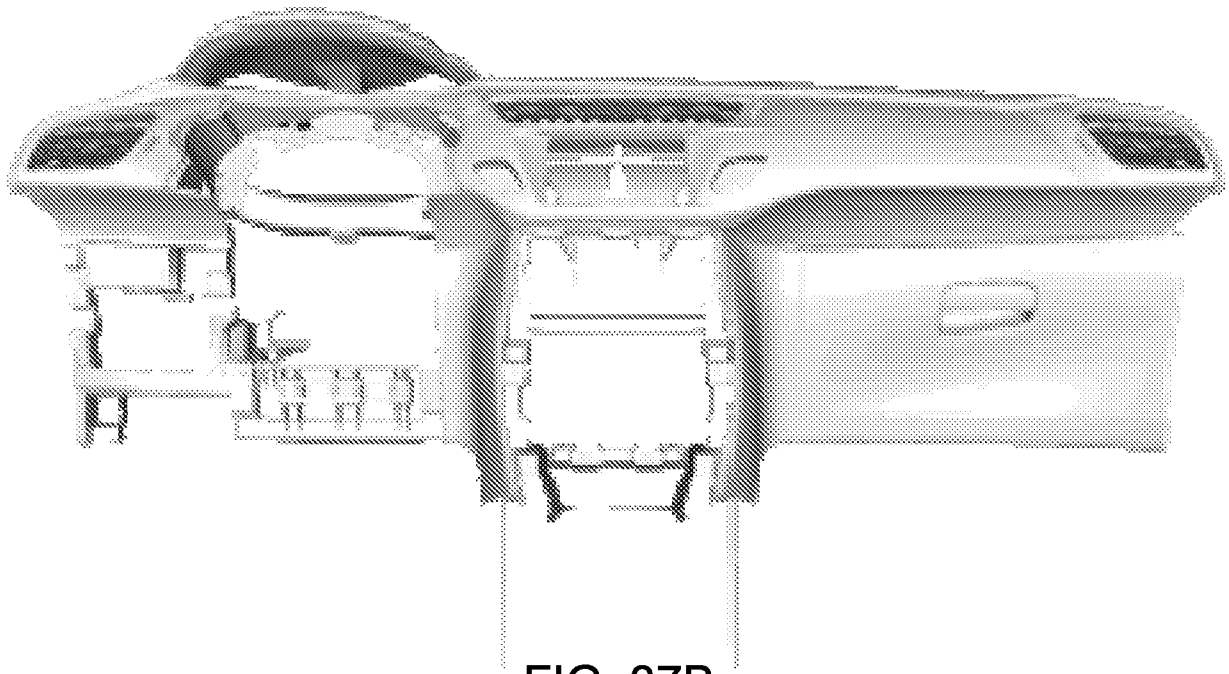

FIG. 37B

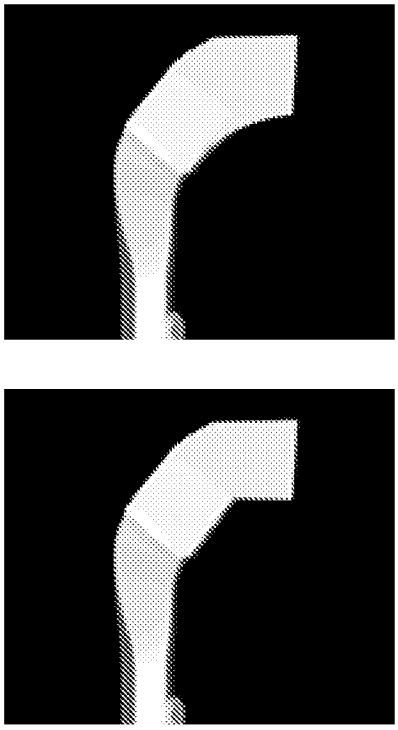

FIG. 38B

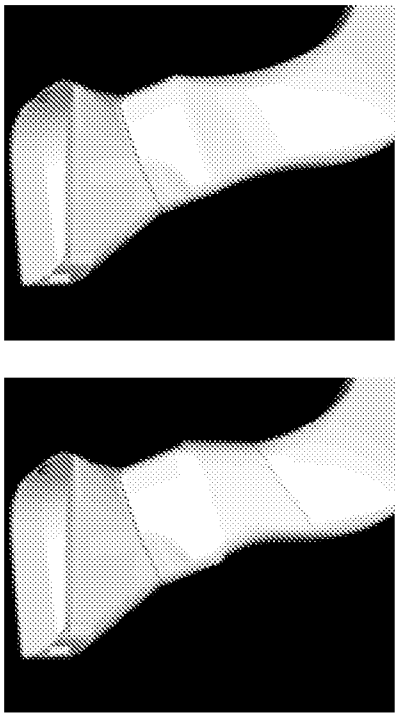

FIG. 38A

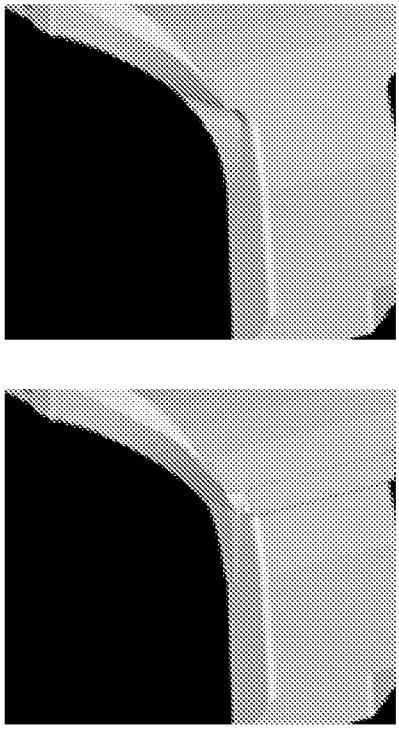

FIG. 39B

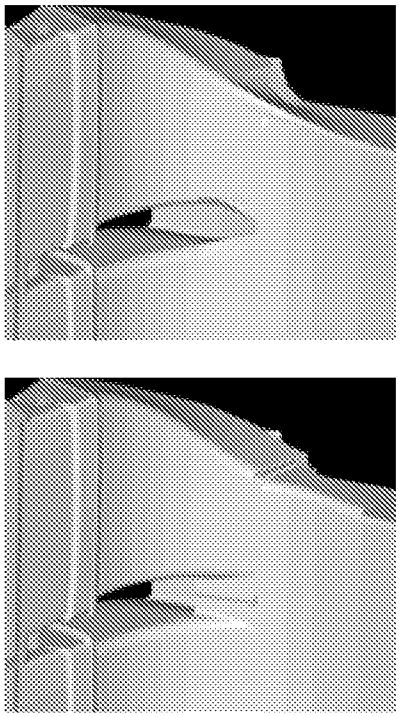

FIG. 39A

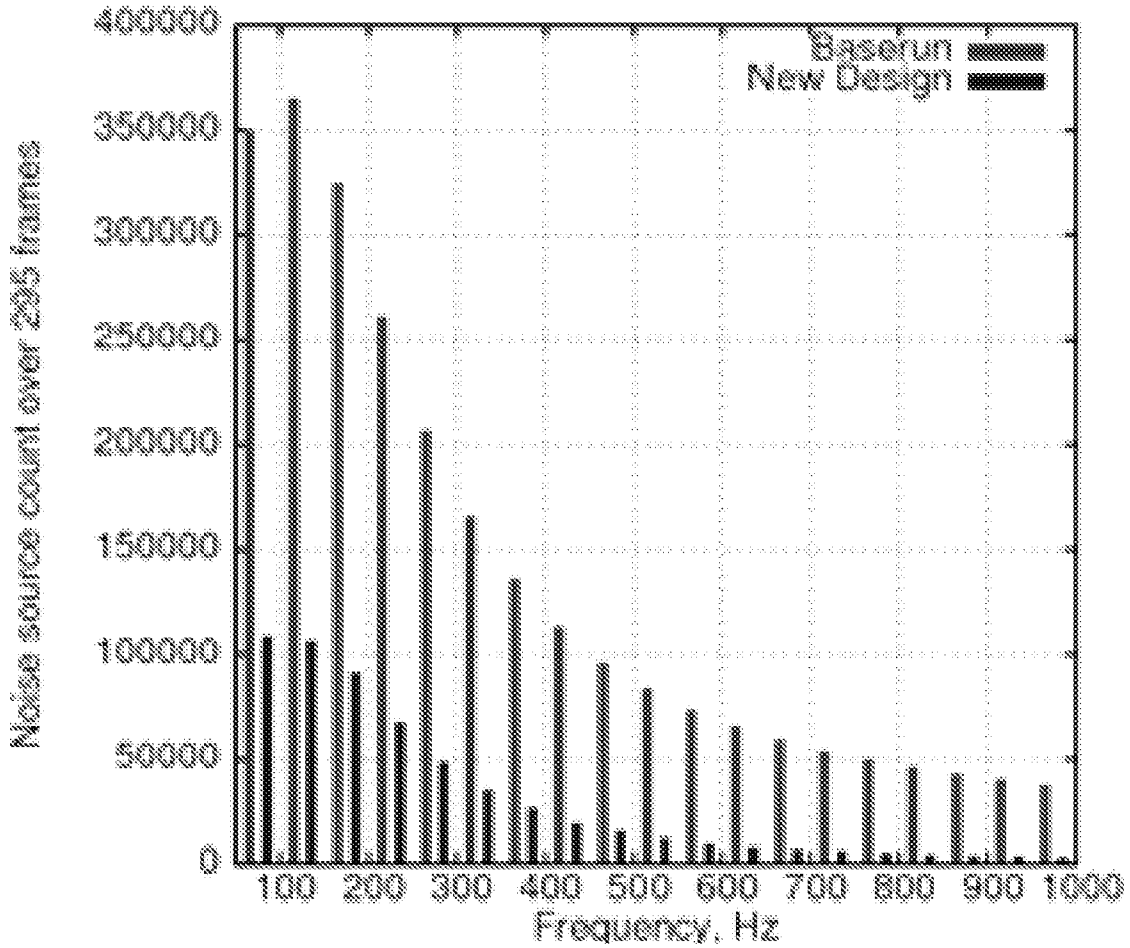
Baserun
New Design
Noise source count over 295 frames
400000
350000
300000
250000
200000
150000
100000
50000
0
100
200
300
400
500
600
700
800
900
1000
Frequency, Hz

FIG. 40

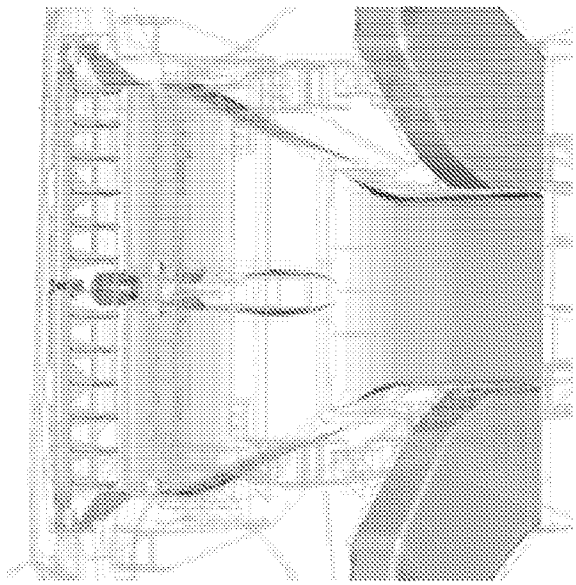

FIG. 41B

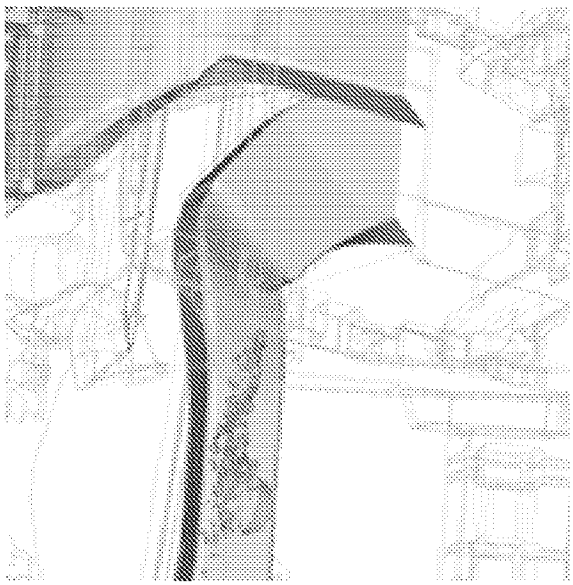

FIG. 42B

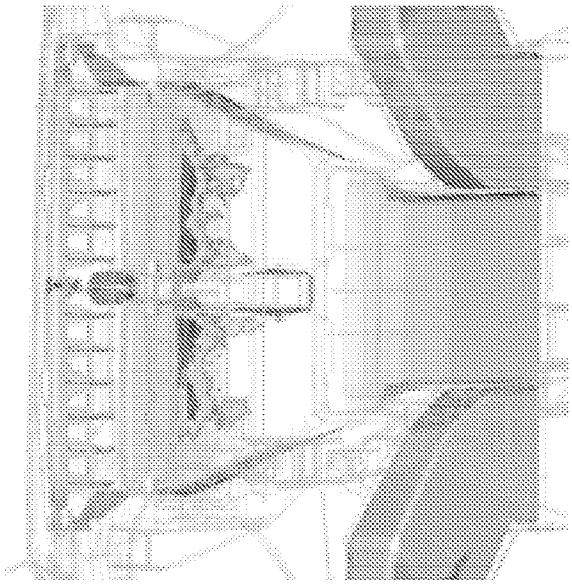

FIG. 41A

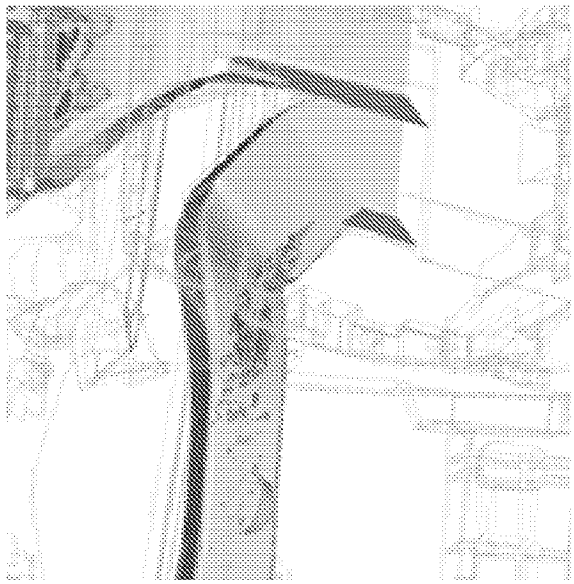

FIG. 42A

INTERNATIONAL SEARCH REPORT

International application No.
PCT/US2014/019074

A. CLASSIFICATION OF SUBJECT MATTER
IPC(8) - G06F19/00 (2014.01)
USPC - 702/50
According to International Patent Classification (IPC) or to both national classification and IPC

B. FIELDS SEARCHED

Minimum documentation searched (classification system followed by classification symbols)
IPC(8) - G06F19/00; G01F1/00; G06G7/57; G06F17/11 (2014.01)
USPC - 702/50, 703/2, 9, 45

Documentation searched other than minimum documentation to the extent that such documents are included in the fields searched
CPC - G06F17/5009; G06F2217/16 (2014.02)

Electronic data base consulted during the international search (name of data base and, where practicable, search terms used)
PatBase, Google Patents, Google Scholar,

C. DOCUMENTS CONSIDERED TO BE RELEVANT

Category*	Citation of document, with indication, where appropriate, of the relevant passages	Relevant to claim No.
Y	US 2011/0144928 A1 (WATANABE et al.) 16 June 2011 (16.06.2011) entire document	1-33
Y	MITCHELL et al. Direct computation of the sound from a compressible co-rotating vortex pair. Research paper. 1995 [retrieved on 2014-05-23]. Retrieved from the internet: <URL: http://journals.cambridge.org/action/displayFulltext?type=1&fid=353446&jid=FLM&volumeId=285&issueId=-1&aid=353444>. entire document	1-33
Y	US 2012/0245903 A1 (STURDZA et al.) 27 September 2012 (27.09.2012) entire document	1-18, 21, 27-33
Y	WO 2001/001237 A1 (DIMAS et al.) 04 January 2001 (04.01.2001) entire document	6, 25, 28
Y	US 5,771,041 A (SMALL) 23 June 1998 (23.06.1998) entire document	12-13, 16-17
Y	US 3,841,587 A (FREED) 15 October 1974 (15.10.1974) entire document	18-26, 32
A	US 2009/0171596 A1 (HOUSTON) 02 July 2009 (02.07.2009) entire document	1-33

☐ Further documents are listed in the continuation of Box C. ☐

* Special categories of cited documents:
"A" document defining the general state of the art which is not considered to be of particular relevance
"E" earlier application or patent but published on or after the international filing date
"L" document which may throw doubts on priority claim(s) or which is cited to establish the publication date of another citation or other special reason (as specified)
"O" document referring to an oral disclosure, use, exhibition or other means
"P" document published prior to the international filing date but later than the priority date claimed
"T" later document published after the international filing date or priority date and not in conflict with the application but cited to understand the principle or theory underlying the invention
"X" document of particular relevance; the claimed invention cannot be considered novel or cannot be considered to involve an inventive step when the document is taken alone
"Y" document of particular relevance; the claimed invention cannot be considered to involve an inventive step when the document is combined with one or more other such documents, such combination being obvious to a person skilled in the art
"&" document member of the same patent family

Date of the actual completion of the international search
23 May 2014

Date of mailing of the international search report
06 JUN 2014

Name and mailing address of the ISA/US
Mail Stop PCT, Attn: ISA/US, Commissioner for Patents
P.O. Box 1450, Alexandria, Virginia 22313-1450
Facsimile No. 571-273-3201

Authorized officer:
Blaine R. Copenheaver
PCT Helpdesk: 571-272-4300
PCT OSP: 571-272-7774

Form PCT/ISA/210 (second sheet) (July 2009)